NAVWEPS REPORT 8772
NOTS TP 3856
COPY 57

NUMERICAL RESULTS FROM THE NOTS LIFTING-SURFACE PROPELLER DESIGN METHOD

by

D. M. Nelson

Underwater Ordnance Department

ABSTRACT. Numerical results from the NOTS lifting-surface propeller design programs are presented. Comparisons of computer solutions with exact analytical solutions are given and indicate that the accuracy of the computer solutions is more than adequate for engineering calculations. Design calculations for a typical wake-adapted propeller are shown. These calculations point out the importance of correctly representing the radial variation of $x \tan\beta$ for a wake-adapted propeller. A discussion is also given of the work presently under way, which will include the effect of the hub boundary condition on lifting-surface propeller design.

U.S. NAVAL ORDNANCE TEST STATION

China Lake, California

August 1965

U. S. NAVAL ORDNANCE TEST STATION

AN ACTIVITY OF THE BUREAU OF NAVAL WEAPONS

J. I. HARDY, CAPT., USN
Commander

WM. B. McLEAN, PH.D.
Technical Director

FOREWORD

This report presents numerical results from lifting-surface propeller design programs. These include comparisons of computer solutions with exact analytical solutions and typical design calculations for a wake-adapted propeller. A discussion of including the hub boundary condition in future design work is also given.

The work was undertaken from August 1963 to April 1965 under Bureau of Naval Weapons Task Assignments R360FR106/2161/R0110101 and RRRE 04001/216 1/R009-01-01. Oscar Seidman was BuWeps project engineer. The purpose of the program was to check the accuracy of the propeller design method presented in NAVWEPS Report 8442, as well as to investigate the important features of the flow induced by a wake-adapted propeller.

The considered opinions of the Propulsion Division are represented in this report.

Released by
J. W. HOYT, Head,
Propulsion Division
26 July 1965

Under authority of
D. J. WILCOX, Head,
Underwater Ordnance
Department

NOTS Technical Publication 3856
NAVWEPS Report 8772

Published by ..... Underwater Ordnance Department
Manuscript 807/MS-164
Collation ..... Cover, 28 leaves, abstract cards
First printing ..... 175 numbered copies
Security classification ..... UNCLASSIFIED

CONTENTS

NOMENCLATURE

C	Chord
C_Q	Torque coefficient, $Q/\frac{1}{2}\rho\pi R^3 v_s^2$
C_T	Thrust coefficient, $T/\frac{1}{2}\rho\pi R^2 v_s^2$
d	Chordwise coordinate measured from leading edge
$d\ell$	Infinitesimal length of vortex line element
D	Propeller diameter
f_0	$\frac{VC}{v_s D} r_R$
$f_1, f_2, \cdots, f_8$	Functions of x (see Eq. 10, Ref.1)
g	Number of blades
G	Nondimensional bound circulation, $\Gamma/\pi D v_s$
Δh	Camber offset divided by the chord
k	Ratio of the strength of a line element of free vorticity at any chordwise station to that at the trailing edge
L	Distance from the stacking line to the leading edge of blade section
M_n	$(\lambda)_{x=x_n}$
N_n	$\left(\frac{d\lambda}{dx}\right)_{x=x_n}$
Q	Torque
r	Radial coordinate
r_R	Ratio of percent thickness of blade section at any spanwise station to percent thickness at reference station
R	Propeller radius
S	Distance from a point on one of the blades to point p
T	Thrust
v	Local axial inflow velocity to propeller
v_δ	Axial inflow velocity to propeller at edge of boundary layer

v_s	Forward speed of propeller relative to undisturbed fluid
V	Relative velocity of blade section and fluid
W	Induced velocity
W_a	Axial component of induced velocity at lifting line
W^*	Apparent axial displacement velocity for an optimum propeller
W_n	Normal component of induced velocity at the lifting line for an optimum propeller
W_t	Tangential component of induced velocity at lifting line
$W_{\bar{Y}}$	Normal component of induced velocity on blade surface
$W_{\underline{Z}}$	Normal component of induced velocity on hub surface
x	Nondimensional radial coordinate, r/R
X, Y, Z	Nondimensional rectangular coordinate system at propeller axis, X = X'/R, etc.
X', Y', Z'	Rectangular coordinate system at propeller axis
$\underline{X}'$, $\underline{Y}'$, $\underline{Z}'$	Rectangular coordinate system having $\underline{Z}'$ axis pass through hub at point p
y	Nondimensional chordwise coordinate, d/C
z	Half-thickness of blade divided by the chord
α	Angle defining points in helical coordinate system
β	Pitch angle of helical sheets
γ	Variation of pitch angle from lifting-line value (ideal angle of attack)
Γ	Bound circulation
$\bar{\Gamma}$	Strength of vortex line element
λ	$x \tan\beta$
λ_s	$v_s/\omega R$
ψ	Angle defining intersection of a helical line and the plane X' = 0
ψ_m	Angles describing stacking-line locations
ω	Angular velocity of propeller

SUBSCRIPTS

B	Due to bound circulation

F Due to free vorticity

h At the hub

p Corresponding to the singularity point on the blade surface or the point on the hub surface where the normal components of induced velocity are calculated

T Due to blade thickness

INTRODUCTION

This report is a follow-up to the author's "A Lifting-Surface Propeller Design Method for High-Speed Computers" (Ref. 1), and presents numerical results from the lifting-surface propeller design computer programs as opposed to the theoretical development given in the earlier work. Since considerable reliance is placed on Ref. 1, and since much the same nomenclature is maintained without extensive explanation of terms, it is assumed that the reader has access to the earlier publication.

Three basic sections make up this report. The first presents check solutions of the lifting-surface propeller design programs. The second presents design calculations for a typical wake-adapted propeller, with particular emphasis on illustrating the effect of operation in a wake in contrast with operation in a uniform stream. The final section outlines changes or additions to the design method which have either been made or are being planned to improve the method and make it more complete.

Interest in the design of propellers by a lifting-surface approach remains high. The works of particular significance which have come to the attention of the author since writing Ref. 1 are those of Kerwin on lifting-surface theory (Ref. 2), Kerwin and Leopold on blade thickness effect (Ref. 3), and Cheng on a lifting-surface design method (Ref. 4) which carries on the work started by Pien (Ref. 5).

CHECK SOLUTIONS OF LIFTING-SURFACE PROPELLER DESIGN COMPUTER PROGRAMS

NEED FOR AND TYPE OF CHECK SOLUTIONS

Since a considerable number of approximations were made in the theoretical development of the lifting-surface design method, it was deemed essential to check computer solutions against exact analytical solutions. This would check not only the adequacy of the approximations used, but also the correctness of the computer programming, a desirable procedure with programs of this complexity.

By allowing the pitch angle, β, of the helical sheets to become either 0° or 90°, the blades become flat surfaces. By choosing certain blade shapes (either rectangular or sector) and certain blade loadings, it was found that exact analytical solutions could be obtained. These are compared with the computer solutions from the bound circulation program, the free vorticity program, and the blade thickness

program. Since the free vorticity program is capable of calculating the lifting-line solution (Page 31, Ref. 1), a comparison with the exact lifting-line solution for an optimum propeller is also shown.

In addition, the ability of the camber line computer program to reproduce a camber line from the slope data is checked by comparisons with some exact solutions for two-dimensional camber lines.

CHECK SOLUTIONS OF BOUND CIRCULATION PROGRAM

The analytical checks of the bound circulation program are presented as Check Solutions 1 - 5. Solutions 1, 3, and 4 show the effect of a blade on itself,[1] while Solutions 2 and 5 show the effect of a surrounding blade.

Since it was not possible to obtain an exact check solution identical to 3 ($\psi_1 = 0$, $\beta = 0°$), but with a variable chordwise loading, and since it was desired to check the ability of the program to handle the variable chordwise loading situation, a nearly exact comparison was made. By choosing a very narrow blade of constant chord, the solution given by the computer program is the one for a nearly rectangular blade. This was compared with the exact solution for a rectangular blade. The comparison is given by Check Solution 4, and was made at only one station near the tip ($x = 0.8$), where the distortion of the blade from a true rectangle would be less.

Check Solution 1. Bound circulation program, effect of blade on itself; comparison of exact analytical solution with computer solution for flat ($\beta = 90°$) rectangular blade.

Hub radius:	$x_h = 0.3$	
Pitch angle:	$\beta = 90°$	flat rectangular blade
Chord:	$C/D = 0.2$	
Blade position:	$\psi_1 = 0.0$	(effect of blade on itself)

Chordwise distribution of bound circulation:

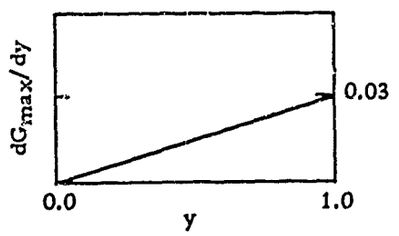

Spanwise distribution of bound circulation:

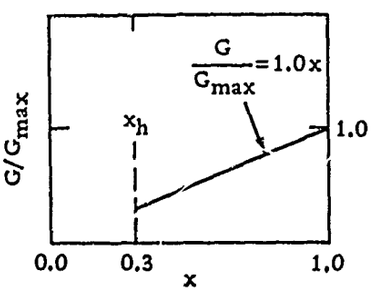

[1] In using the term "the effect of a blade on itself," reference is made to the velocity induced at a point on a blade due to the singularity distribution representing that blade. Use of the term "the effect of a surrounding blade" refers to the velocity induced at a point on a blade due to the singularity distribution representing another blade.

TABLE 1. Comparison of Exact and Computer Solutions for Check Solution 1

Error (based on values rounded to five places): where the absolute error exceeds 0.00001, the percent error is less than 0.043%.

y_p	$(W\bar{Y}/v_s)_B$									
	$x_p = 0.35$		$x_p = 0.50$		$x_p = 0.65$		$x_p = 0.80$		$x_p = 0.95$	
	Computer	Exact	Computer	Exact	Computer	Exact	Computer	Exact	Computer	Exact
-0.05	-0.01770	-0.01770	-0.02712	-0.02712	-0.03408	-0.03408	-0.03754	-0.03754	-0.03194	-0.03194
0.05	-0.02503	-0.02502	-0.03865	-0.03865	-0.04923	-0.04922	-0.05599	-0.05599	-0.05111	-0.05110
0.15	-0.02768	-0.02767	-0.04328	-0.04328	-0.05543	-0.05543	-0.06363	-0.06363	-0.05824	-0.05823
0.25	-0.02808	-0.02807	-0.04434	-0.04434	-0.05700	-0.05699	-0.06580	-0.06580	-0.06014	-0.06013
0.35	-0.02691	-0.02691	-0.04280	-0.04280	-0.05519	-0.05519	-0.06410	-0.06410	-0.05877	-0.05875
0.45	-0.02431	-0.02430	-0.03882	-0.03882	-0.05020	-0.05020	-0.05878	-0.05877	-0.05446	-0.05445
0.55	-0.02013	-0.02013	-0.03216	-0.03215	-0.04170	-0.04170	-0.04943	-0.04942	-0.04690	-0.04688
0.65	-0.01402	-0.01401	-0.02215	-0.02215	-0.02882	-0.02882	-0.03491	-0.03491	-0.03503	-0.03502
0.75	-0.00506	-0.00506	-0.00732	-0.00731	-0.00965	-0.00965	-0.01278	-0.01277	-0.01635	-0.01634
0.85	0.00926	0.00926	0.01612	0.01612	0.02072	0.02072	0.02316	0.02317	0.01629	0.01630
0.95	0.04104	0.04103	0.06485	0.06485	0.08395	0.08395	0.09977	0.09977	0.09663	0.09659
1.05	0.05035	0.05034	0.07909	0.07908	0.10230	0.10230	0.12151	0.12151	0.11858	0.11853

TABLE 1. Comparison of Exact and Computer Solutions for Check Solution 1

Error (based on values rounded to five places): where the absolute error exceeds 0.00001, the percent error is less than 0.043%.

y_p	$(W\overline{Y}/v_s)_B$									
	$x_p = 0.35$		$x_p = 0.50$		$x_p = 0.65$		$x_p = 0.80$		$x_p = 0.95$	
	Computer	Exact	Computer	Exact	Computer	Exact	Computer	Exact	Computer	Exact
-0.05	-0.01770	-0.01770	-0.02712	-0.02712	-0.03408	-0.03408	-0.03754	-0.03754	-0.03194	-0.03194
0.05	-0.02503	-0.02502	-0.03865	-0.03865	-0.04923	-0.04922	-0.05599	-0.05599	-0.05111	-0.05110
0.15	-0.02768	-0.02767	-0.04328	-0.04328	-0.05543	-0.05543	-0.06363	-0.06363	-0.05824	-0.05823
0.25	-0.02808	-0.02807	-0.04434	-0.04434	-0.05700	-0.05699	-0.06580	-0.06580	-0.06014	-0.06013
0.35	-0.02691	-0.02691	-0.04280	-0.04280	-0.05519	-0.05519	-0.06410	-0.06410	-0.05877	-0.05875
0.45	-0.02431	-0.02430	-0.03882	-0.03882	-0.05020	-0.05020	-0.05878	-0.05877	-0.05446	-0.05445
0.55	-0.02013	-0.02013	-0.03216	-0.03215	-0.04170	-0.04170	-0.04943	-0.04942	-0.04690	-0.04688
0.65	-0.01402	-0.01401	-0.02215	-0.02215	-0.02882	-0.02882	-0.03491	-0.03491	-0.03503	-0.03502
0.75	-0.00506	-0.00506	-0.00732	-0.00731	-0.00965	-0.00965	-0.01278	-0.01277	-0.01635	-0.01634
0.85	0.00926	0.00926	0.01612	0.01612	0.02072	0.02072	0.02316	0.02317	0.01629	0.01630
0.95	0.04104	0.04103	0.06485	0.06485	0.08395	0.08395	0.09977	0.09977	0.09663	0.09659
1.05	0.05035	0.05034	0.07909	0.07908	0.10230	0.10230	0.12151	0.12151	0.11858	0.11853

Check Solution 2. Bound circulation program, effect of a surrounding blade; comparison of exact analytical solution with computer solution for flat ($\beta = 90°$) rectangular blade.

Hub radius:	$x_h = 0.3$	
Pitch angle:	$\beta = 90°$	flat rectangular blade
Chord:	$C/D = 0.2$	
Blade position:	$\psi_2 = 0.7$ radians (effect of a surrounding blade)	

Chordwise distribution of bound circulation:

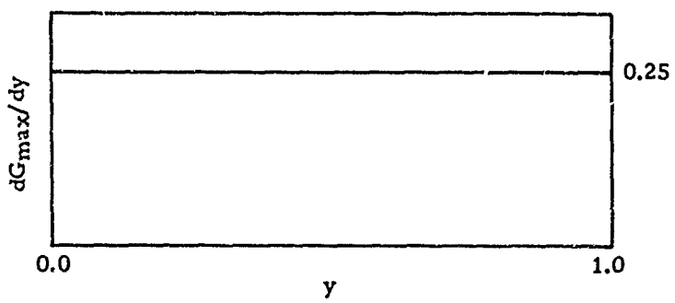

Spanwise distribution of bound circulation:

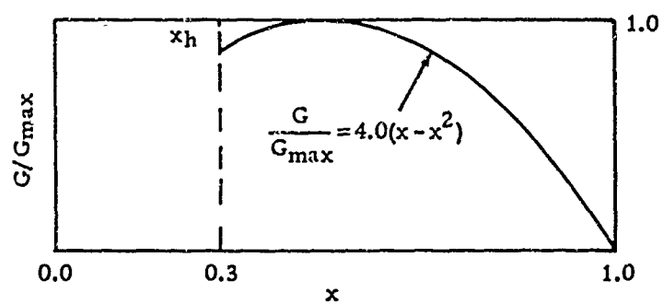

TABLE 2. Comparison of Exact and Computer Solutions for Check Solution 2

Error (based on values rounded to five places): where the absolute error exceeds 0.00001, the percent error is less than 0.048%.

y_p	$(W\bar{Y}/v_s)_B$									
	$x_p = 0.35$		$x_p = 0.50$		$x_p = 0.65$		$x_p = 0.80$		$x_p = 0.95$	
	Computer	Exact	Computer	Exact	Computer	Exact	Computer	Exact	Computer	Exact
-0.05	-0.12756	-0.12760	-0.10480	-0.10484	-0.07353	-0.07355	-0.04829	-0.04831	-0.03106	-0.03107
0.05	-0.11540	-0.11543	-0.09350	-0.09352	-0.06452	-0.06454	-0.04175	-0.04177	-0.02653	-0.02654
0.15	-0.09695	-0.09698	-0.07793	-0.07795	-0.05311	-0.05313	-0.03397	-0.03398	-0.02137	-0.02138
0.25	-0.07313	-0.07315	-0.05860	-0.05861	-0.03961	-0.03962	-0.02511	-0.02511	-0.01568	-0.01568
0.35	-0.04540	-0.04542	-0.03637	-0.03638	-0.02446	-0.02446	-0.01542	-0.01542	-0.00958	-0.00958
0.45	-0.01539	-0.01539	-0.01233	-0.01233	-0.00827	-0.00827	-0.00520	-0.00520	-0.00322	-0.00322
0.55	0.01539	0.01539	0.01233	0.01233	0.00827	0.00827	0.00520	0.00520	0.00322	0.00322
0.65	0.04540	0.04542	0.03637	0.03638	0.02446	0.02446	0.01542	0.01542	0.00958	0.00958
0.75	0.07313	0.07315	0.05860	0.05861	0.03961	0.03962	0.02511	0.02511	0.01568	0.01568
0.85	0.09695	0.09698	0.07793	0.07795	0.05311	0.05313	0.03397	0.03398	0.02137	0.02138
0.95	0.11540	0.11543	0.09350	0.09352	0.06452	0.06454	0.04175	0.04177	0.02653	0.02654
1.05	0.12756	0.12760	0.10480	0.10484	0.07353	0.07355	0.04829	0.04831	0.03106	0.03107

Check Solution 3 Bound circulation program, effect of blade on itself; comparison of exact analytical solution with computer solution for flat ($\beta = 0°$) sector-shaped blade.

Hub radius:	$x_h = 0.3$	
Pitch angle:	$\beta = 0°$	} flat sector-shape blade
Chord:	$C/D = 0.3x$	} flat sector-shape blade
Blade position:	$\psi_1 = 0.0$ (effect of blade on itself)	

Chordwise distribution of bound circulation:

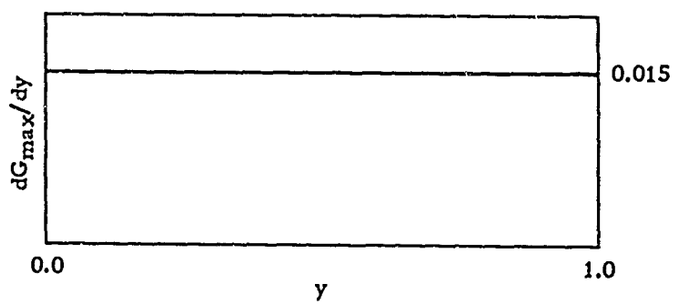

Spanwise distribution of bound circulation:

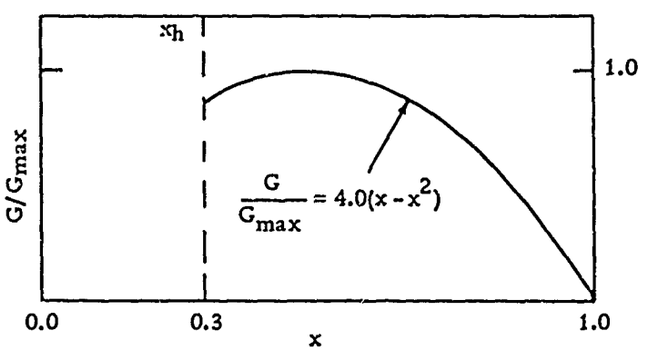

TABLE 3. Comparison of Exact and Computer Solutions for Check Solution 3

Error (based on values rounded to five places): where the absolute error exceeds 0.00001, the percent error is less than 0.060%.

y_p	$(W_{\overline{Y}}/v_s)_B$									
	$x_p = 0.35$		$x_p = 0.50$		$x_p = 0.65$		$x_p = 0.80$		$x_p = 0.95$	
	Computer	Exact	Computer	Exact	Computer	Exact	Computer	Exact	Computer	Exact
-0.05	-0.15982	-0.15990	-0.13612	-0.13617	-0.09572	-0.09574	-0.05645	-0.05644	-0.02293	-0.02292
0.05	-0.15667	-0.15675	-0.13309	-0.13313	-0.09344	-0.09346	-0.05488	-0.05487	-0.02188	-0.02187
0.15	-0.08407	-0.08412	-0.07524	-0.07527	-0.05291	-0.05292	-0.03151	-0.03151	-0.01457	-0.01457
0.25	-0.05032	-0.05035	-0.04647	-0.04648	-0.03273	-0.03274	-0.01970	-0.01971	-0.00980	-0.00980
0.35	-0.02743	-0.02744	-0.02578	-0.02578	-0.01818	-0.01819	-0.01103	-0.01103	-0.00570	-0.00570
0.45	-0.00875	-0.00876	-0.00829	-0.00829	-0.00585	-0.00586	-0.00356	-0.00356	-0.00187	-0.00187
0.55	0.00875	0.00876	0.00829	0.00829	0.00585	0.00586	0.00356	0.00356	0.00187	0.00187
0.65	0.02743	0.02744	0.02578	0.02578	0.01818	0.01819	0.01103	0.01103	0.00570	0.00570
0.75	0.05032	0.05035	0.04647	0.04648	0.03273	0.03274	0.01970	0.01971	0.00980	0.00980
0.85	0.08407	0.08412	0.07524	0.07527	0.05291	0.05292	0.03151	0.03151	0.01457	0.01457
0.95	0.15667	0.15675	0.13309	0.13313	0.09344	0.09346	0.05488	0.05487	0.02188	0.02187
1.05	0.15982	0.15990	0.13612	0.13617	0.09572	0.09574	0.05645	0.05644	0.02293	0.02292

Check Solution 4. Bound circulation program, effect of blade on itself; comparison of exact analytical solution for flat, rectangular blade with computer solution for flat ($\beta = 0°$) "near"-rectangular blade.

Hub radius:	$x_h = 0.3$	
Pitch angle:	$\beta = 0°$	} flat, "near"-rectangular blade
Chord:	$C/D = 0.05$	}
Blade position:	$\psi_1 = 0.0$ (effect of blade on itself)	

Chordwise distribution of bound circulation:

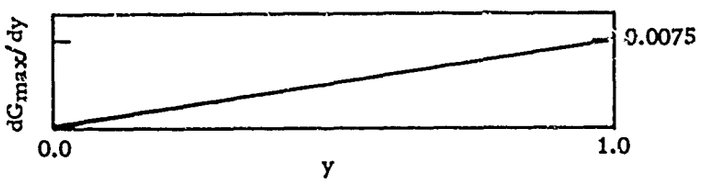

Spanwise distribution of bound circulation:

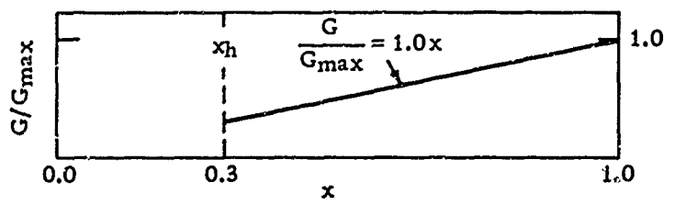

TABLE 4. Comparison of Exact and Computer Solutions for Solution 4

Error: not computed since comparison is not exact.

y_p	$(W\overline{Y}/v_s)_B$	
	$x_p = 0.80$	
	Computer	Exact
-0.1	-0.04372	-0.04374
0.1	-0.07174	-0.07175
0.3	-0.07429	-0.07429
0.5	-0.05961	-0.05956
0.7	-0.02464	-0.02450
0.9	0.05783	0.05804
1.1	0.09717	0.09714

Check Solution 5. Bound circulation program, effect of a surrounding blade; comparison of exact analytical solution with computer solution for a flat ($\beta = 0°$) sector-shaped blade.

Hub radius:	$x_h = 0.3$	
Pitch angle:	$\beta = 0.0°$	flat sector-shaped blade
Chord:	$C/D = 0.3x$	
Blade position:	$\psi_2 = 0.7$ radians (effect of a surrounding blade)	

Chordwise distribution of bound circulation:

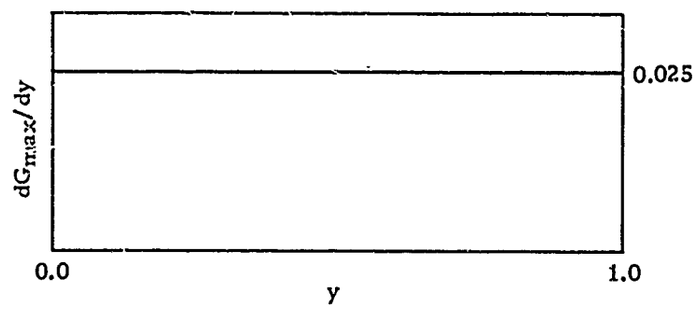

Spanwise distribution of bound circulation:

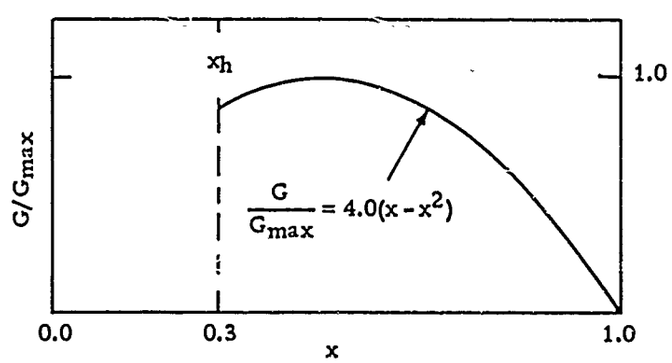

TABLE 5. Comparison of Exact and Computer Solutions for Check Solution 5

Error (based on values rounded to five places): where the absolute error exceeds 0.00001, the percent error is less than 0.062%.

y_p	$(W\bar{Y}/v_s)_B$									
	$x_p = 0.35$		$x_p = 0.50$		$x_p = 0.65$		$x_p = 0.80$		$x_p = 0.95$	
	Computer	Exact	Computer	Exact	Computer	Exact	Computer	Exact	Computer	Exact
-0.05	-0.02253	-0.02254	-0.02091	-0.02092	-0.01662	-0.01663	-0.01259	-0.01259	-0.00946	-0.00946
0.05	-0.02528	-0.02529	-0.02360	-0.02361	-0.01861	-0.01862	-0.01392	-0.01393	-0.01030	-0.01030
0.15	-0.02853	-0.02854	-0.02680	-0.02681	-0.02095	-0.02096	-0.01545	-0.01546	-0.01125	-0.01125
0.25	-0.03242	-0.03244	-0.03065	-0.03066	-0.02373	-0.02374	-0.01723	-0.01724	-0.01231	-0.01231
0.35	-0.03716	-0.03718	-0.03534	-0.03535	-0.02708	-0.02709	-0.01933	-0.01933	-0.01350	-0.01351
0.45	-0.04303	-0.04305	-0.04114	-0.04115	-0.03117	-0.03118	-0.02182	-0.02183	-0.01486	-0.01487
0.55	-0.05048	-0.05051	-0.04844	-0.04845	-0.03626	-0.03627	-0.02486	-0.02486	-0.01642	-0.01642
0.65	-0.06022	-0.06025	-0.05784	-0.05786	-0.04275	-0.04276	-0.02863	-0.02864	-0.01824	-0.01824
0.75	-0.07349	-0.07353	-0.07033	-0.07035	-0.05132	-0.05133	-0.03351	-0.03352	-0.02039	-0.02039
0.85	-0.09267	-0.09272	-0.08770	-0.08772	-0.06321	-0.06322	-0.04017	-0.04017	-0.02302	-0.02302
0.95	-0.12306	-0.12313	-0.11380	-0.11383	-0.08111	-0.08113	-0.05011	-0.05011	-0.02644	-0.02644
1.05	-0.18010	-0.18020	-0.15988	-0.15993	-0.11294	-0.11295	-0.06782	-0.06782	-0.03158	-0.03157

CHECK SOLUTIONS OF FREE VORTICITY PROGRAM

The analytical checks of the free vorticity program are given as Check Solutions 6 - 9. Solutions 6 and 8 show the effect of a blade on itself, while Solutions 7 and 9 show the effect of a surrounding blade.

Since the angle, α (see Fig. 1, Ref. 1), which is the independent variable when integrating over the free vorticity sheets (see Eq. 35, Ref. 1), is undefined when $\beta = 90°$, it was necessary to make β almost equal to 90° in Check Solutions 6 and 7, rather than exactly 90°. In Solution 6, $x \tan\beta$ was made equal to 120 and in Solution 7 it was made equal to 1,000. Further, since the upper limit of integration in the free vorticity program is determined by an axial distance behind the point where the velocity is desired (see discussion, Page 30, Ref. 1), it was necessary to make β almost equal to 0° in Solutions 8 and 9, rather than exactly 0°. In these solutions, $x \tan\beta$ was made equal to 0.001.

The chordwise variation of the free vorticity is given in terms of k, the ratio of the strength of an element of free vorticity, $\bar{\Gamma}$, at any chordwise station, to the strength at the trailing edge, $\bar{\Gamma}_{TE}$. It is related to the chordwise loading distribution, as discussed on Pages 26 and 27 of Ref. 1.

It was possible to obtain an exact solution for only one value of y_p with Check Solutions 7, 8, and 9.

Check Solution 6. Free vorticity program, effect of blade on itself; comparison of exact analytical solution with computer solution for a flat ($\beta = 90°$) rectangular blade.

Hub radius:	$x_h = 0.3$	
Pitch angle:	$\beta = 90°$	flat rectangular blade
Chord:	$C/D = 0.1$	
Blade position:	$\psi_t = 0.0$	(effect of blade on itself)

Chordwise variation of $k = \bar{\Gamma}/\bar{\Gamma}_{TE}$:

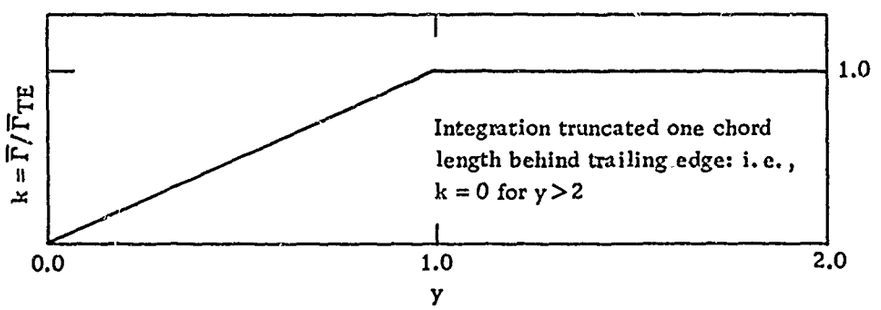

Spanwise variation of bound circulation:

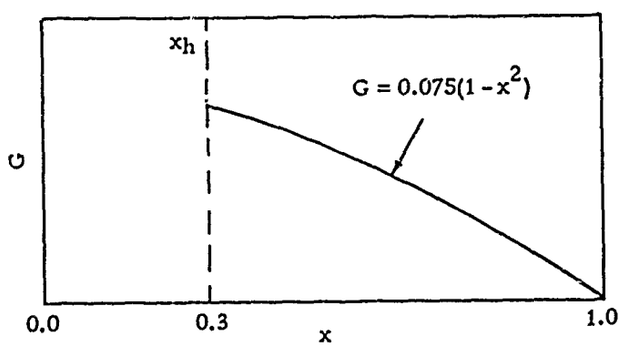

TABLE 6. Comparison of Exact and Computer Solutions for Check Solution 6

Error (based on values rounded to five places): where the absolute error exceeds 0.00001, the percent error is less than 0.020%.

y_p	$(W\overline{Y}/v_s)_F$							
	$x_p = 0.35$		$x_p = 0.55$		$x_p = 0.75$		$x_p = 0.95$	
	Computer	Exact	Computer	Exact	Computer	Exact	Computer	Exact
-0.05	0.04441	0.04441	0.03012	0.03012	0.00332	0.00332	-0.04908	-0.04908
0.05	0.0511	0.05110	0.03446	0.03446	0.00562	0.00561	-0.05758	-0.05758
0.15	0.05914	0.05913	0.03967	0.03967	0.00874	0.00874	-0.06729	-0.06728
0.25	0.06798	0.06798	0.04531	0.04531	0.01228	0.01228	-0.07817	-0.07816
0.35	0.07730	0.07729	0.05118	0.05118	0.01607	0.01607	-0.08983	-0.08982
0.45	0.08679	0.08678	0.05712	0.05712	0.01999	0.01999	-0.10186	-0.10185
0.55	0.09623	0.09622	0.06299	0.06299	0.02394	0.02394	-0.11388	-0.11387
0.65	0.10537	0.10536	0.06866	0.06865	0.02784	0.02783	-0.12550	-0.12548
0.75	0.11396	0.11394	0.07398	0.07397	0.03156	0.03156	-0.13632	-0.13631
0.85	0.12170	0.12168	0.07878	0.07878	0.03501	0.03501	-0.14591	-0.14589
0.95	0.12822	0.12820	0.08286	0.08285	0.03799	0.03798	-0.15383	-0.15380
1.05	0.13294	0.13292	0.08574	0.08573	0.04006	0.04005	-0.15998	-0.15995

Check Solution 7. Free vorticity program, effect of a surrounding blade; comparison of exact analytical solution with computer solution for a flat ($\beta = 90°$) rectangular blade.

Hub radius:	$x_h = 0.3$	
Pitch angle:	$\beta = 90°$	} flat rectangular blade
Chord:	$C/D = 0.2$	}
Blade position:	$\psi_2 = 0.7$ radians (effect of a surrounding blade)	

Chordwise variation of $k = \overline{\Gamma}/\overline{\Gamma}_{TE}$:

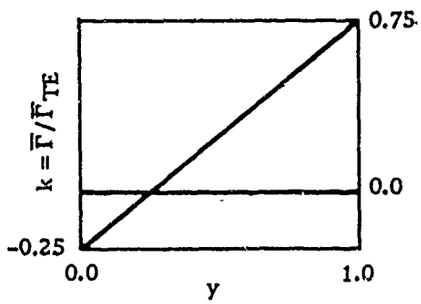

(Integration truncated at the trailing edge; i.e., $k = 0$ for $y > 1$)

Spanwise variation of bound circulation:

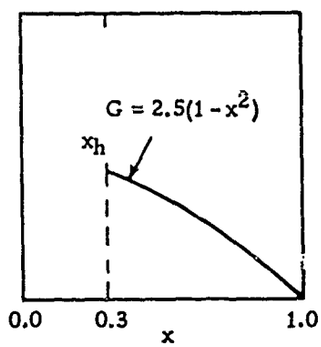

TABLE 7. Comparison of Exact and Computer Solutions for Check Solution 7

Error (based on values rounded to five places): where the absolute error exceeds 0.00001, the percent error is less than 0.068%.

x_p	$(W_{\overline{Y}}/v_s)_{\overline{F}}$	
	$y_p = 0.25$	
	Computer	Exact
0.35	0.07345	0.07347
0.45	-0.00478	-0.00479
0.55	-0.06817	-0.06821
0.65	-0.11211	-0.11218
0.75	-0.13763	-0.13772
0.85	-0.14781	-0.14790
0.95	-0.14662	-0.14672

Check Solution 8. Free vorticity program, effect of a blade on itself; comparison of exact analytical solution with computer solution for a flat ($\beta = 0°$) sector-shaped blade.

Hub radius:	$x_h = 0.3$	
Pitch angle:	$\beta = 0°$	flat sector-shaped blade
Chord:	$C/D = 0.3x$	
Blade position:	$\psi_1 = 0.0$ (effect of a blade on itself)	

Chordwise variation of $k = \overline{\Gamma}/\overline{\Gamma}_{TE}$:

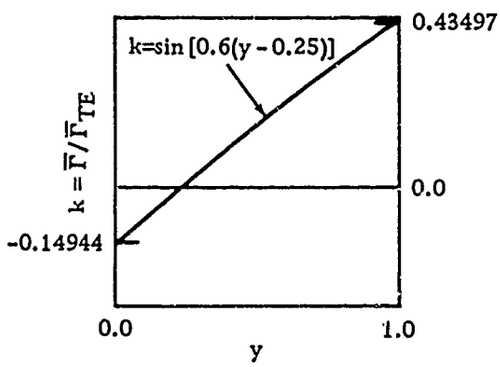

(Integration truncated at trailing edge; i.e., k=0 for y > 1)

Spanwise variation of bound circulation:

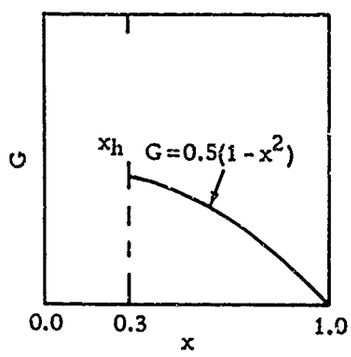

TABLE 8. Comparison of Exact and Computer Solutions for Check Solution 8

Error (based on values rounded to five places): maximum absolute error of 0.00001.

x_p	$(W_{\overline{Y}}/v_s)_F$	
	$y_p = 0.25$	
	Computer	Exact
0.35	0.10362	0.10363
0.45	0.09368	0.09368
0.55	0.07994	0.07994
0.65	0.05979	0.05979
0.75	0.03221	0.03221
0.85	-0.00085	-0.00085
0.95	-0.03057	-0.03057

Check Solution 8. Free vorticity program, effect of a blade on itself; comparison of exact analytical solution with computer solution for a flat ($\beta = 0°$) sector-shaped blade.

Hub radius: $x_h = 0.3$
Pitch angle: $\beta = 0°$
Chord: $C/D = 0.3x$ } flat sector-shaped blade
Blade position: $\psi_1 = 0.0$ (effect of a blade on itself)

Chordwise variation of $k = \overline{\Gamma}/\overline{\Gamma}_{TE}$:

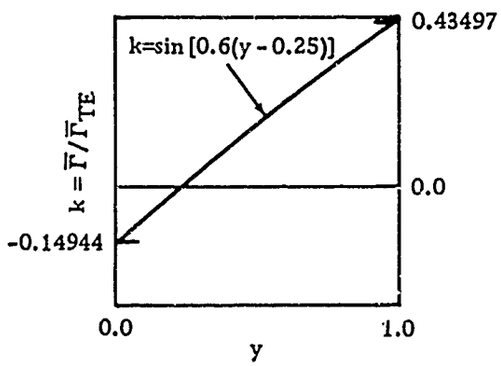

(Integration truncated at trailing edge; i.e., k=0 for y > 1)

Spanwise variation of bound circulation:

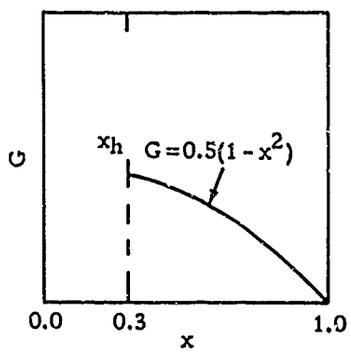

TABLE 8. Comparison of Exact and Computer Solutions for Check Solution 8

Error (based on values rounded to five places): maximum absolute error of 0.00001.

x_p	$(W\overline{\gamma}/v_s)_F$	
	$y_p = 0.25$	
	Computer	Exact
0.35	0.10362	0.10363
0.45	0.09368	0.09368
0.55	0.07994	0.07994
0.65	0.05979	0.05979
0.75	0.03221	0.03221
0.85	-0.00085	-0.00085
0.95	-0.03057	-0.03057

Check Solution 9. Free vorticity program, effect of a surrounding blade; comparison of exact analytical solution with computer solution for a flat ($\beta = 0°$) sector-shaped blade.

Hub radius:	$x_h = 0.3$	
Pitch angle:	$\beta = 0°$	} flat sector-shaped blade
Chord:	$C/D = 0.3x$	
Blade position:	$\psi_2 = 0.7$ radians (effect of a surrounding blade)	

Chordwise variation of $k = \bar{\Gamma}/\bar{\Gamma}_{TE}$:

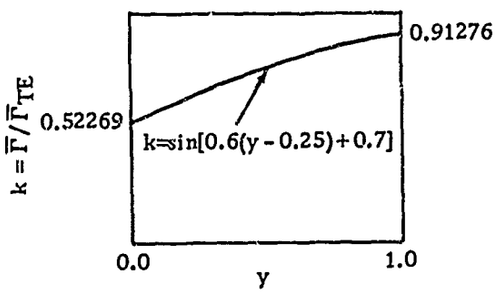

(Integration truncated at trailing edge; i.e., k=0 for y > 1)

Spanwise variation of bound circulation:

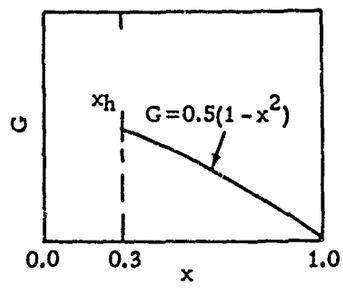

TABLE 9. Comparison of Exact and Computer Solutions for Check Solution 9

Error (based on values rounded to five places): maximum absolute error of 0.00001.

x_p	$(W\bar{\gamma}/v_s)_F$	
	$y_p = 0.25$	
	Computer	Exact
0.35	0.19990	0.19991
0.45	0.16718	0.16719
0.55	0.13030	0.13031
0.65	0.09468	0.09469
0.75	0.06337	0.06337
0.85	0.03811	0.03811
0.95	0.01940	0.01940

CHECK SOLUTIONS OF BLADE THICKNESS PROGRAM

Since the component of velocity normal to a plane source sheet at a point on the sheet[2] is zero, check solutions of the blade thickness program for the effect of a blade on itself for flat blades ($\beta = 0°$ or $90°$) yield trivial solutions of zero. It was therefore not possible to obtain meaningful check solutions for the effect of a blade on itself, so that in this case extensive hand calculations to check out the computer programs had to be made. However, it was possible to obtain check solutions for the case of the effect of a surrounding blade. Check Solution 10 presents such a comparison for the case $\beta = 90°$. An exact solution was possible at only one value of y_p.

For the effect of a surrounding blade and $\beta = 0°$, trivial solutions of zero also appear, since all the blades fall in one plane. However, it happened that the blade thickness program was so written that it could also obtain the component of velocity along the blade $W_{\bar{x}}$ (see Fig. 2, Ref. 1) for this particular case. A comparison of values of $W_{\bar{x}}$ is given by Check Solution 11 for $\beta = 0°$.

---

[2] Not at an infinitesimal distance on either side.

Check Solution 10. Blade thickness program, effect of a surrounding blade; comparison of exact analytical solution with computer solution for a flat ($\beta = 90°$) rectangular blade.

Hub radius:	$x_h = 0.3$	
Pitch angle:	$\beta = 90°$	flat rectangular blade
Chord:	$C/D = 0.2$	
Blade position:	$\psi_2 = 0.7$ radians (effect of a surrounding blade)	

Chordwise variation of blade thickness:

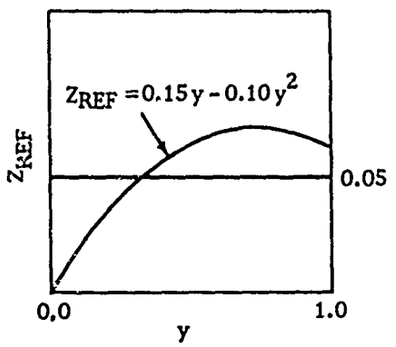

Spanwise variation of f_0:

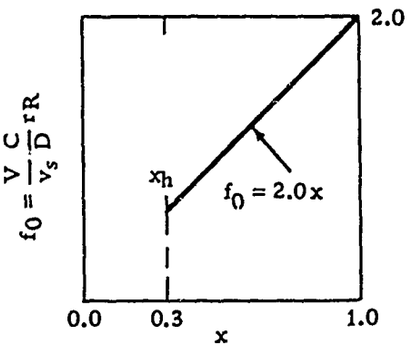

(See pp. 36 - 38 of Ref. 1 for explanation of Z_{REF} and f_0)

TABLE 10. Comparison of Exact and Computer Solutions for Check Solution 10

Error: maximum absolute error less than 0.00001.

x_p	$(W_{\bar{Y}}/v_s)_T$	
	$y_p = 0.75$	
	Computer	Exact
0.35	0.04762	0.04762
0.45	0.04845	0.04845
0.55	0.04540	0.04540
0.65	0.04012	0.04012
0.75	0.03386	0.03386
0.85	0.02756	0.02756
0.95	0.02185	0.02185

Check Solution 11. Blade thickness program, effect of a surrounding blade on the velocity along (not normal to) the blade, comparison exact analytical solution with computer solution for a flat ($\beta = 0°$) sector-shaped blade.

Hub radius:	$x_h = 0.3$	
Pitch angle:	$\beta = 0°$	flat sector-shaped blade
Chord:	$C/D = 0.3x$	
Blade position:	$\psi_2 = 0.7$ radians (effect of surrounding blade)	

Chordwise variation of blade thickness:

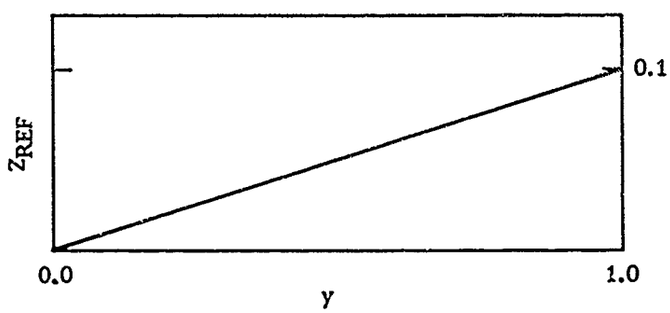

Spanwise variation of f_0:

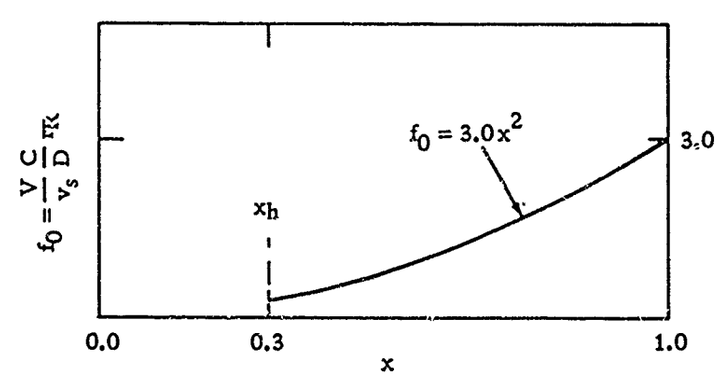

(See pages 36 - 38 of Ref. 1 for explanation of Z_{REF} and f_0)

TABLE 11. Comparison of Exact and Computer Solutions for Check Solution 11

Error (based on values rounded to five places): maximum percent error of 0.063%.

y_p	$(W_{\overline{X}}/v_s)_T$							
	$x_p = 0.35$		$x_p = 0.55$		$x_p = 0.75$		$x_p = 0.95$	
	Computer	Exact	Computer	Exact	Computer	Exact	Computer	Exact
-0.05	-0.08579	-0.08582	-0.06968	-0.06969	-0.04897	-0.04898	-0.03910	-0.03910
0.05	-0.09279	-0.09282	-0.07793	-0.07795	-0.05552	-0.05553	-0.03600	-0.03600
0.15	-0.10049	-0.10052	-0.08758	-0.08759	-0.06340	-0.06341	-0.04091	-0.04091
0.25	-0.10900	-0.10903	-0.09892	-0.09894	-0.07301	-0.07302	-0.04687	-0.04687
0.35	-0.11846	-0.11850	-0.11240	-0.11242	-0.08491	-0.08492	-0.05424	-0.05424
0.45	-0.12911	-0.12915	-0.12857	-0.12860	-0.09991	-0.09992	-0.06352	-0.06351
0.55	-0.14126	-0.14132	-0.14823	-0.14827	-0.11922	-0.11924	-0.07552	-0.07551
0.65	-0.15550	-0.15556	-0.17259	-0.17264	-0.14473	-0.14475	-0.09156	-0.09155
0.75	-0.17286	-0.17293	-0.20356	-0.20362	-0.17955	-0.17957	-0.11400	-0.11398
0.85	-0.19541	-0.19549	-0.24462	-0.24470	-0.22924	-0.22929	-0.14761	-0.14758
0.95	-0.22800	-0.22811	-0.30338	-0.30349	-0.30539	-0.30546	-0.20394	-0.20388
1.05	-0.28552	-0.28570	-0.40265	-0.40280	-0.44059	-0.44072	-0.32211	-0.32198

CHECK OF LIFTING-LINE SOLUTION BY FREE VORTICITY PROGRAM

The free vorticity program is capable of calculating the lifting-line solution, as discussed on Page 31 of Ref. 1. Hence an additional check on the program was made by a comparison with the exact lifting-line solution for an optimum propeller.

Figure 1 shows the bound circulation distribution presented in the form

$$\frac{g\Gamma\omega}{2\pi W^*(v_s + W^*)}$$

versus x for a four-bladed optimum propeller, as computed by Goldstein (Ref. 6) from the motion of rigid helical sheets. By a law established by Betz (Ref. 7), the fluid motion in the ultimate wake of an optimum propeller is such that the shed vorticity sheets form true

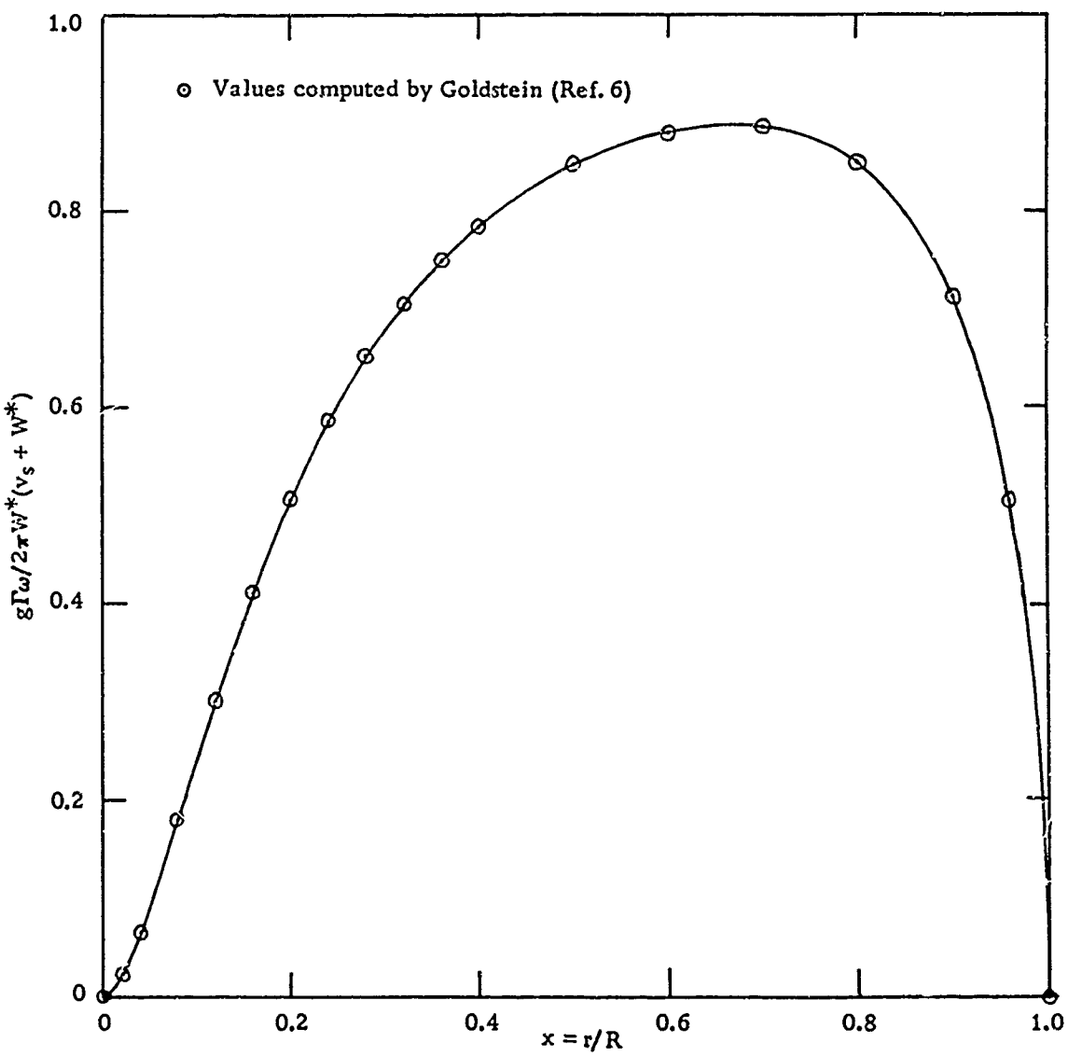

FIG. 1. Optimum Circulation Distribution for Four-Bladed Propeller.

helical sheets, and hence move as if they were rigid with an apparent axial displacement velocity, denoted here by W^*. Since the free vorticity sheets form true helical sheets, they can be described by the two coordinates r and $\theta = \psi + \alpha - (X'/r \tan\beta)$ (see Fig. 1, Ref. 1). θ is a constant on any true helical surface of pitch, $2\pi r \tan\beta$. For an axial motion of the true helical sheets, the boundary condition is a function of only r and θ. Therefore the potential generated by the motion of the helical sheets is also a function of only r and θ, and there are no velocities induced along the sheets, since the coordinate describing position in that direction is everywhere perpendicular to the coordinates r and θ. Thus the resultant of the axial and tangential components of induced velocity on the shed vorticity sheets is normal to the sheets. This is the normality condition for optimum propellers.

Following Lerbs (Ref. 8) in applying the Betz condition and normality at the lifting line, the nondimensional bound circulation, $G = \Gamma/\pi D v_s$, is related to Goldstein's circulation function given in Fig. 1 by

$$G = \frac{2\lambda_s[1 + (W^*/v_s)]}{g} \frac{W^*}{v_s} \left[\frac{g\Gamma\omega}{2\pi W^*(v_s + W^*)}\right] \qquad (1)$$

where $\lambda_s = v_s/\omega R$. Further, the relative flow vector diagram at the lifting line takes the form shown in Fig. 2, so that the normal component of

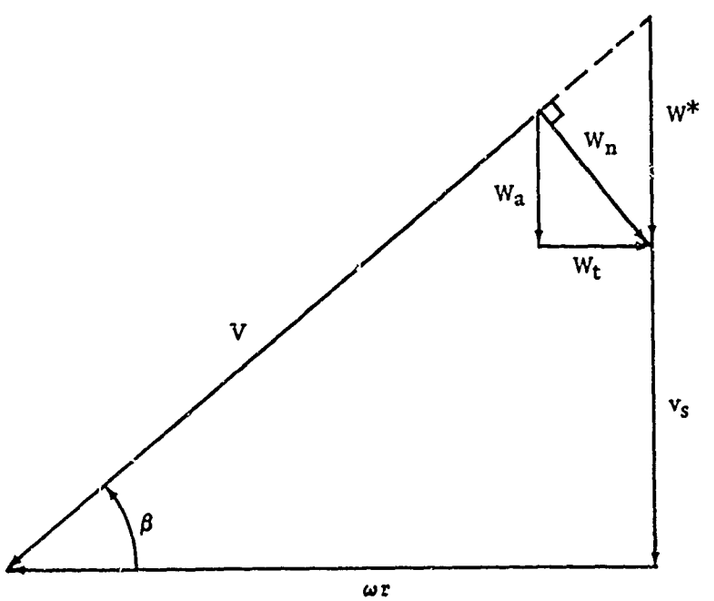

FIG. 2. Optimum Propeller Velocity Diagram at the Lifting Line.

induced velocity, W_n, which is equivalent to the component $(W\bar{Y})_F$ computed by the free vorticity program, is given by

$$\frac{W_n}{v_s} = \frac{W^*}{v_s} \frac{x}{\sqrt{x^2 + \lambda_s^2[1 + (W^*/v_s)]^2}} \tag{2}$$

and the pitch of the helical sheets is given by

$$x \tan\beta = \lambda_s \left(1 + \frac{W^*}{v_s}\right) \tag{3}$$

The bound circulation distribution and pitch distribution given by Eq. 1 and 3 for values of $\lambda_s = 0.16$ and $W^*/v_s = 0.25$ were used in the free vorticity computer program to calculate the normal component of induced velocity. These values are compared with the exact values given by Eq. 2 in Fig. 3.

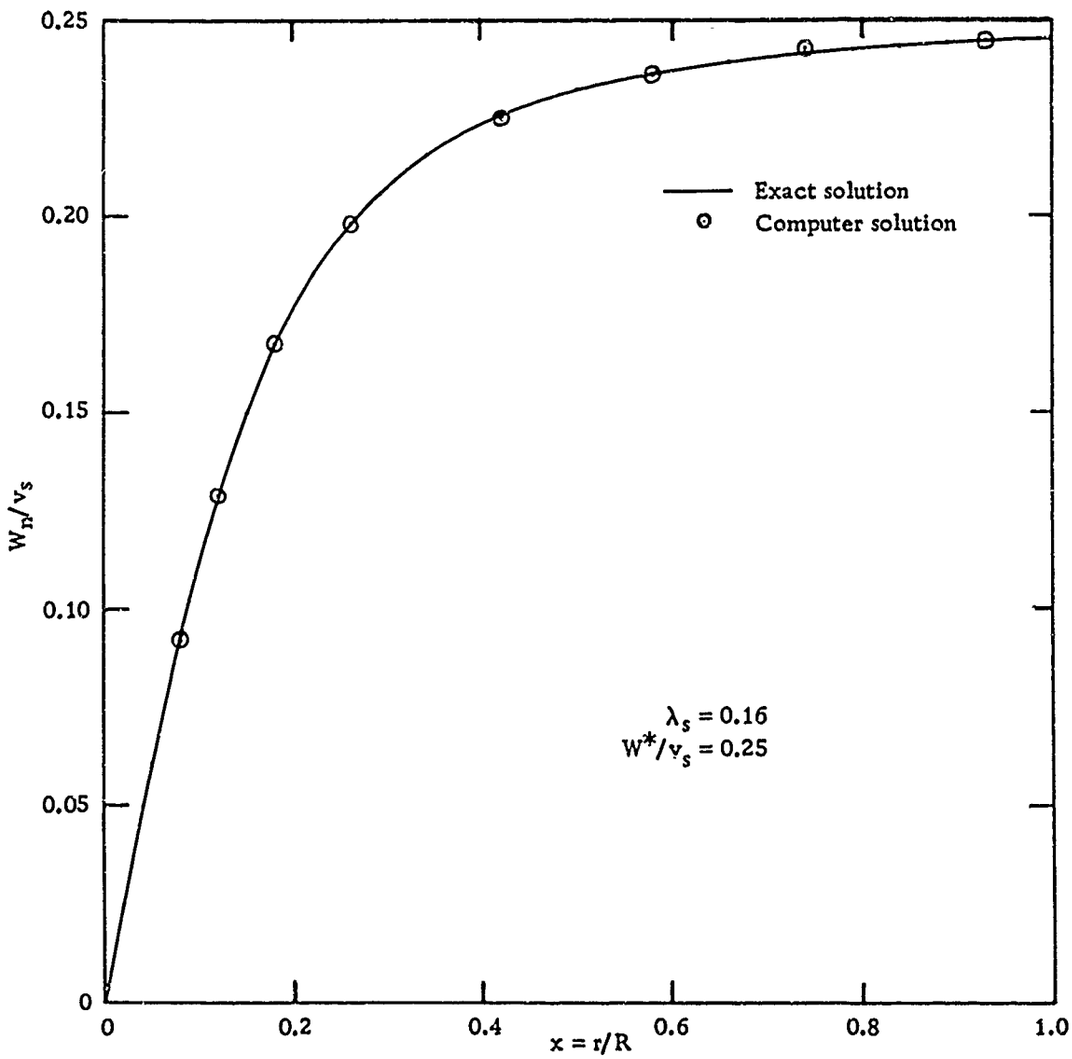

FIG. 3. Comparison of Exact Solution With Solution Given by the Free Vorticity Computer Program for the Normal Component of Induced Velocity at the Lifting Line for a Four-Bladed Optimum Propeller.

CHECK SOLUTIONS OF CAMBER LINE PROGRAM

The camber line computer program uses a polynomial fit to the camber line slope data to reproduce the camber line and its orientation in the flow. Since the accuracy of such a procedure for typical camber lines was not known, comparisons with exact solutions for two-dimensional camber lines were made. The camber lines for two cases of trapezoidal chordwise loading (Ref. 9) were used. (Trapezoidal chordwise loadings have been adopted at NOTS as the best for marine propellers, and will be discussed later.) One of the loadings is symmetric about the center of the blade; the other is not. Values of the camber line slope from the exact solution corresponding to y = -0.05, 0.05, 0.15, 0.25, 0.35, 0.45, 0.55, 0.65, 0.75, 0.85, 0.95, and 1.05 were input to the computer program.[3] The computed camber lines and ideal angles of attack are compared with the exact solutions in Fig. 4 and 5.

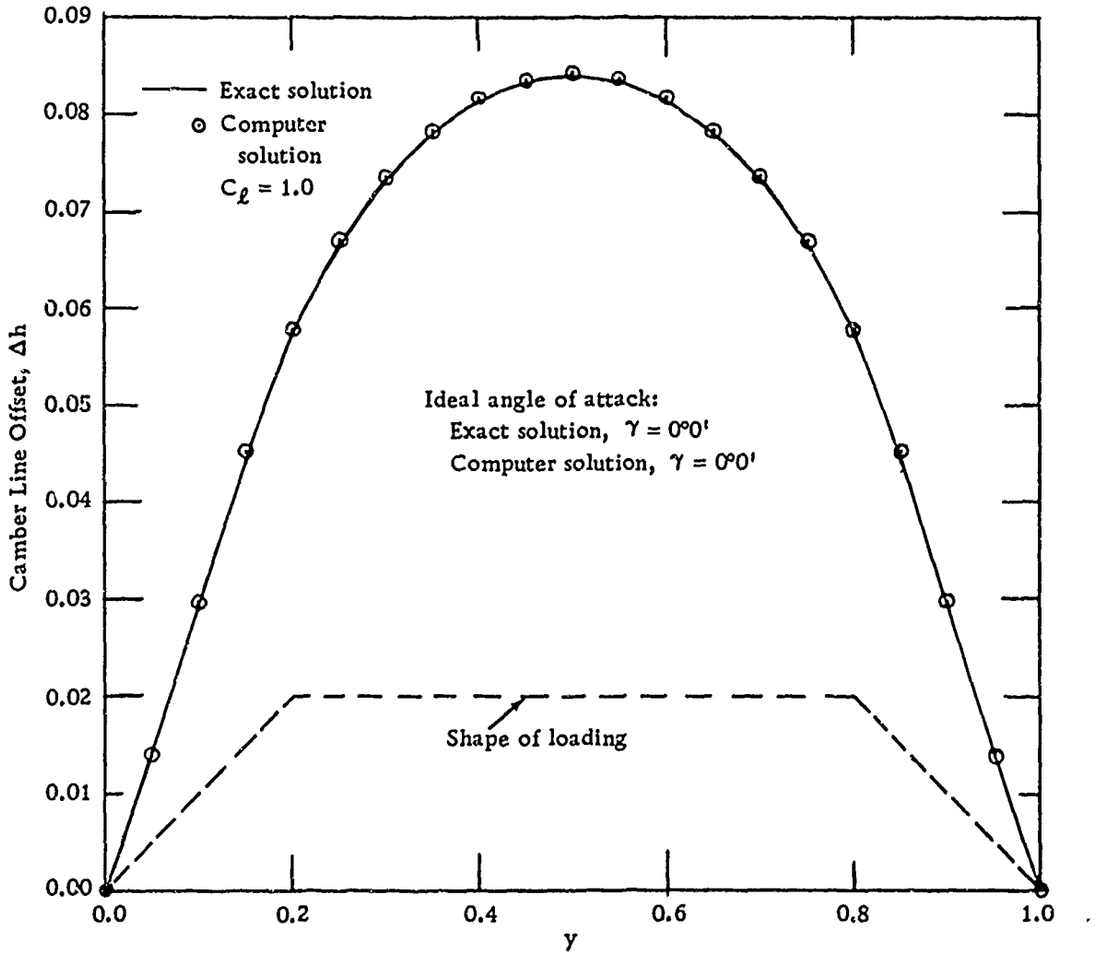

FIG. 4. Comparison of Exact Solution With Solution Given by the Camber Line Computer Program for a Two-Dimensional Airfoil With Symmetric Trapezoidal Loading.

[3] See section on modifications to the camber line computer program below.

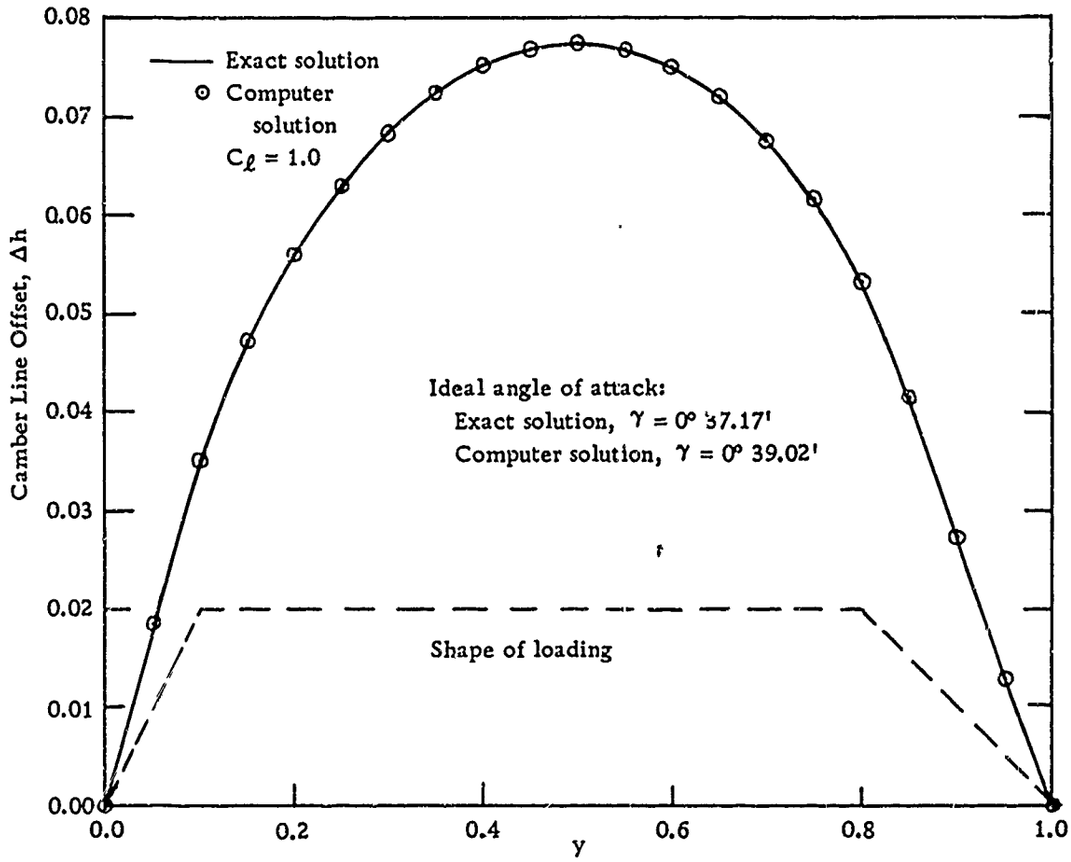

FIG. 5. Comparison of Exact Solution With Solution Given by the Camber Line Computer Program for a Two-Dimensional Airfoil With Unsymmetric Trapezoidal Loading.

ACCURACY OF COMPUTER PROGRAM SOLUTIONS

The comparisons of the exact solutions with the corresponding computer solutions (Check Solutions 1 - 3 and 5 - 11) given by the bound circulation, free vorticity, and blade thickness programs, show that where the absolute errors in the nondimensional normal component of induced velocity exceed 0.00001, the percent errors are less than 0.068%. This level of accuracy does not represent the maximum attainable by the programs but rather that which may be arrived at by a compromise with computing time. This area is discussed in the Appendix. The accuracy of these solutions should be reasonably indicative of that which is obtained in actual propeller design calculations, and is certainly more than adequate for engineering calculations.

In the comparison of the free vorticity program solution with the exact solution for the normal component of velocity at the lifting line of a four-bladed optimum propeller (Fig. 3), the maximum error was 0.765%. Considering the number and distribution of the points available

from Goldstein's calculations for defining the bound circulation distribution (Fig. 1), it is probably unreasonable to expect better agreement.

Comparisons of the camber lines and ideal angles of attack computed by the camber line program with those given by the exact solution (Fig. 4 and 5) show the following: For the symmetrical loading, the ideal angle of attack was given exactly, and the camber offsets had a maximum error of 1.20% of the maximum offset; for the unsymmetrical loading, the ideal angle of attack was in error by 1.85 minutes of arc, and the camber offsets had a maximum error of 0.94% of the maximum offset. For torpedo propellers, errors of this magnitude will normally give rise to noncritical inaccuracies in locating points on the blade surface. Since these propellers are always relatively small and moderately loaded, these errors are no larger than the manufacturing tolerances that presently prevail. Hence the camber line program should be adequate for engineering design calculations.

TYPICAL WAKE-ADAPTED PROPELLER DESIGN CALCULATIONS

SPECIFICATIONS

The following specifications were assumed for the propeller design:

1. Develop a thrust coefficient, $C_T = 0.1$
2. Operate at an advance ratio, $\lambda_s = 0.5$
3. Operate at a Reynolds number based on the propeller diameter and free stream velocity, $Dv_s/\nu = 5.0 \times 10^6$
4. Utilize five blades
5. Have a hub radius, $r_h = 0.3R$
6. Operate free of cavitation for $P_{DEPTH} - P_{VAPOR}/\frac{1}{2}\rho v_s^2 \geq 0.85$

WAKE PROFILE

At NOTS, the principal interest is in propellers for torpedoes. These are located at the end of a tapering afterbody, where the wake profile is normally that of a turbulent boundary layer. The boundary layer profiles can usually be approximated fairly closely by a power law, a typical value of the power being 1/5. Assuming that the tip of the propeller coincides with the edge of the boundary layer, a typical wake profile will be given by

$$\frac{v}{v_\delta} = \left(\frac{r - r_h}{R - r_h}\right)^{1/5}$$

Since $x_h = r_h/R = 0.3$ for the propeller considered here,

$$\frac{v}{v_\delta} = \left(\frac{x - 0.3}{0.7}\right)^{1/5} \tag{4}$$

It is further assumed that the velocity at the edge of the boundary layer is 0.95 of the free stream velocity, i. e.,

$$\frac{v_\delta}{v_s} = 0.95 \tag{5}$$

BLADE THICKNESS DISTRIBUTION

The 10% NACA 63A thickness distribution (i. e., NACA 63A 010) at the hub is chosen for the propeller blades. The distribution at all other blade stations is derived from NACA 63A 010 by shrinking all the thickness coordinates proportionally to provide a linear variation in the thickness from 10% at the hub to 6% at the tip. Hence the nondimensional half-thickness of the blades as a function of the nondimensional radial and chordwise coordinates is given by

$$z = r_R(x)f(y) \tag{6}$$

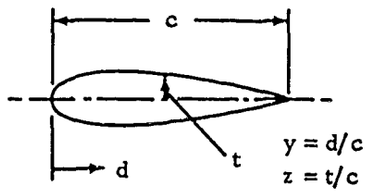

where $r_R = 1.17143 - 0.57143x$ and where f(y) describes the variation of z versus y for the NACA 63A 010 distribution.

It is advantageous to decrease the percent thickness from hub to tip as indicated above, since this reduces the overvelocities due to thickness near the tip, where the higher relative velocity of blade section and fluid tends to make them larger. However, this advantage must be weighed against the disadvantage arising because the thinner blade sections have larger overvelocities due to off-design angles of attack.

CIRCULATION DISTRIBUTION

For a wake-adapted propeller operating in a turbulent boundary layer-type wake, the spanwise (or radial) variation of bound circulation should be one that has its maximum value near the hub. Such a bound circulation variation accelerates the slow-moving fluid by the greatest amount, resulting in higher efficiency. Furthermore, since a single-rotating propeller is being considered here, the circulation distribution must go to zero at the hub. Experience has shown that if the propeller is designed to maintain circulation there, the accompanying mean tangential velocities give rise to a strong and highly cavitation-prone hub vortex behind the propeller. As a consequence of the above two requirements, a typical spanwise circulation

distribution for the type of propeller considered here is shown in Fig. 6. This circulation distribution was adopted for the present study.

Note in Fig. 6 that the circulation does not drop to zero exactly at the hub, but rather at a point a small distance from it where the inflow velocity to the propeller (Eq.4 and 5) is still relatively large compared to the free stream velocity. Because the inflow velocity drops to zero at the hub, a circulation distribution that does not drop to zero at that point is dictated by both physical and theoretical considerations. First of all, it is physically impossible to twist the blade rapidly enough to follow the relative flow velocity vector in the region very near the hub. Second, viscous effects predominate in the boundary layer flow there, so that the potential flow considerations used in propeller design are probably nonvalid. Hence it becomes necessary to exclude in the design calculations a small region of the flow near the hub by defining an effective hub radius where the circulation drops to zero. Even ignoring the above argument, strictly theoretical considerations make such a procedure necessary. If a lifting-line solution using Lerbs' induction factor method (Ref. 8) is attempted for the propeller, where the circulation and inflow velocity drop to zero at the same radial location, a solution normally cannot be obtained. The first time through, the calculation of the induced velocities gives rise to negative ones and hence negative values of β near the hub (see Fig. 1, Ref. 1) because the inflow velocity is so small there. These negative values of β imply the absurd condition that the flow at that location moves upstream rather than downstream. The first iteration on the induced velocities with these negative values of β near the hub gives rise to positive induced velocities and positive values of β there. Subsequent iterations oscillate between negative and positive values of β, and no solution is obtained.

Chordwise distributions of bound circulation of the trapezoidal type (see Fig. 7) have been adopted at NOTS as the best for propeller design. Chordwise loadings of this type go to zero at the trailing edge, so that the Kutta condition is satisfied and, consequently, viscous corrections to lift are not large. These loadings also go to zero at the leading edge, so that the over-velocity due to lift is small in that area, where a spike may occur owing to possible off-design angles of attack. Hence better cavitation performance is expected from these loadings. The actual chordwise loading used in this study (Fig. 7) was chosen to be symmetric about the center of the blade. Some interesting features of this arrangement will be explored elsewhere in the report.

VARIATION OF CHORD WITH SPAN

A preliminary run of the Lerbs' induction factor lifting-line program, neglecting viscous drag of the blades, was made to obtain a reasonable estimate of G_{max} and the induced velocities. These values, together with the inflow velocity profile given by Eq. 4 and 5, the blade thickness distribution given by Eq. 6, and the spanwise and chordwise distribution of bound circulation shown in Fig. 6 and 7, were utilized to calculate the minimum value of C/D versus x to meet the requirement

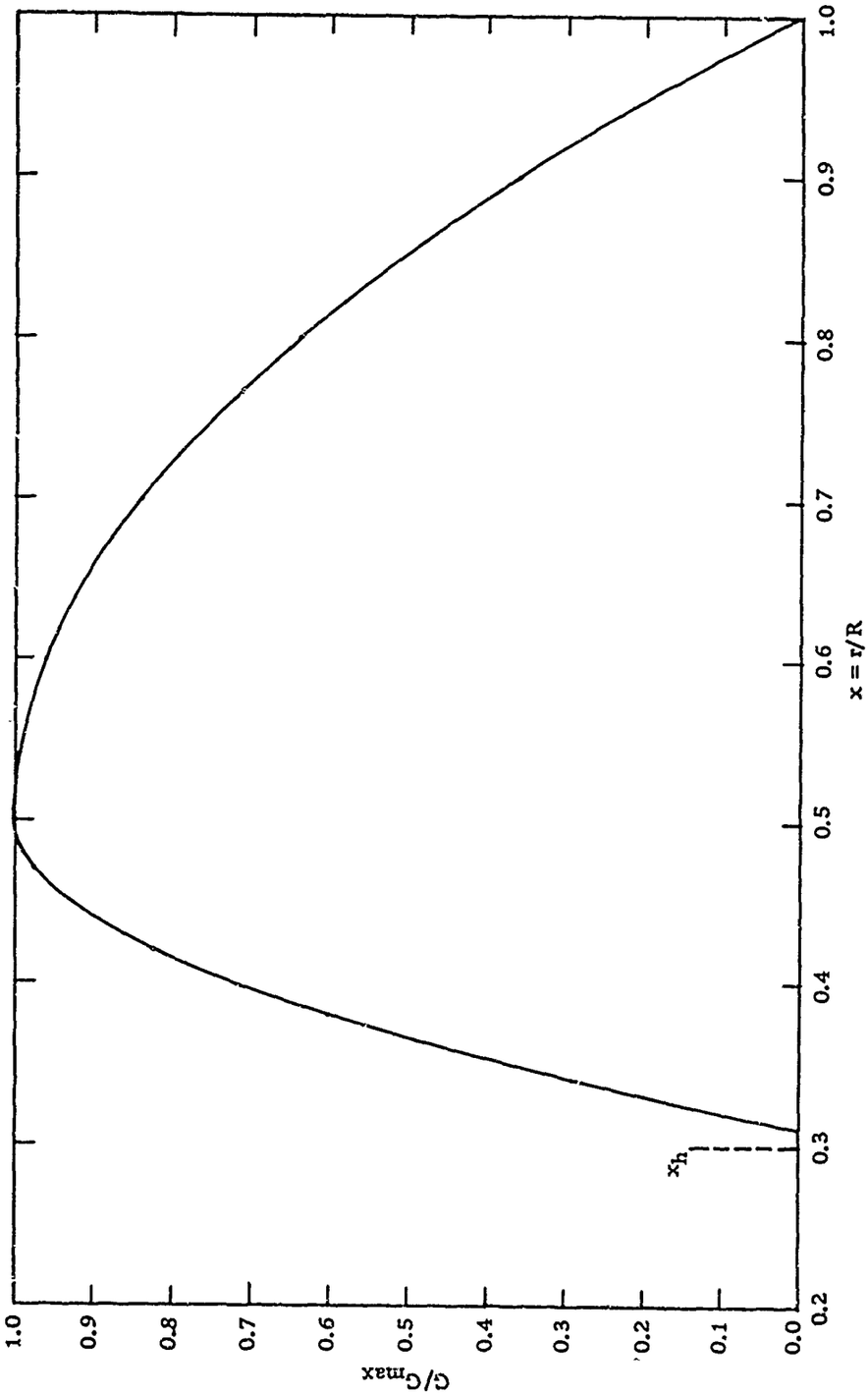

FIG. 6. Spanwise Variation of Bound Circulation.

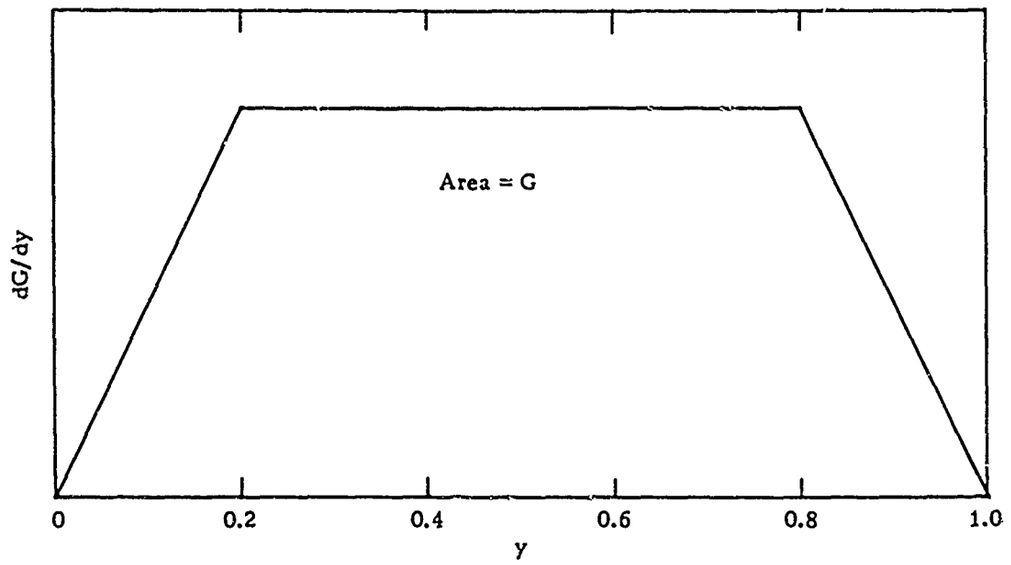

FIG. 7. Chordwise Variation of Bound Circulation.

of cavitation-free operation for $P_{DEPTH} - P_{VAPOR} / \frac{1}{2}\rho v_s^2 \geq 0.85$. In these calculations, the variation of static pressure through the propeller was accounted for and the usual assumption that the static pressure is a constant across a boundary layer was made. Since calculations of this type are common in propeller design, no details are given here. A plot of the minimum value of C/D versus x to meet the cavitation requirement is shown in Fig. 8. The actual C/D versus x chosen is also shown, and it is seen that some margin was left for possible off-design conditions.

LERBS' LIFTING-LINE SOLUTION

As discussed on Pages 2 and 3 of Ref. 1, Lerbs' induction factor lifting-line solution (Ref. 8) serves as a starting point for applying the lifting-surface solution. It yields the pitch distribution of the helical sheets upon which the singularity distributions representing the lifting surfaces are placed. It also yields the magnitude of the bound circulation needed to meet the thrust requirement. The lifting-line computer program uses a slightly extended version of Lerbs' induction factor method, in which the drag of the blade section is accounted for in computing the thrust and torque of the propeller. Using the inflow velocity profile given by Eq. 4 and 5, the spanwise variation of bound circulation shown in Fig. 6, the spanwise variation of chord shown in Fig. 8, the required thrust coefficient $C_T = 0.1$, and the required advance ratio $\lambda_s = 0.5$ as inputs to the lifting-line computer program, the spanwise variation of axial and tangential induced velocities at the lifting line shown in Fig. 9 were calculated. The required maximum value of the bound circulation ($G_{max} = 0.00967$) and the torque ($C_Q = 0.0543$) to generate the desire thrust also were given by the program. In this

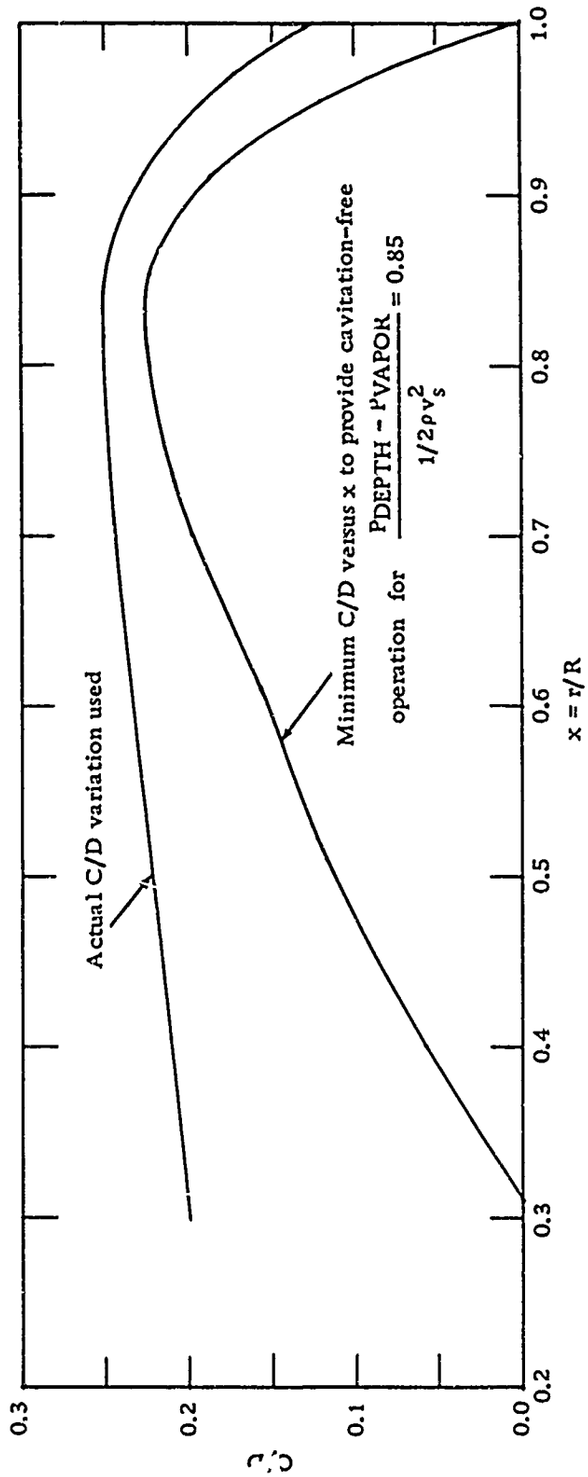

FIG. 8. Spanwise Variation of Chord.

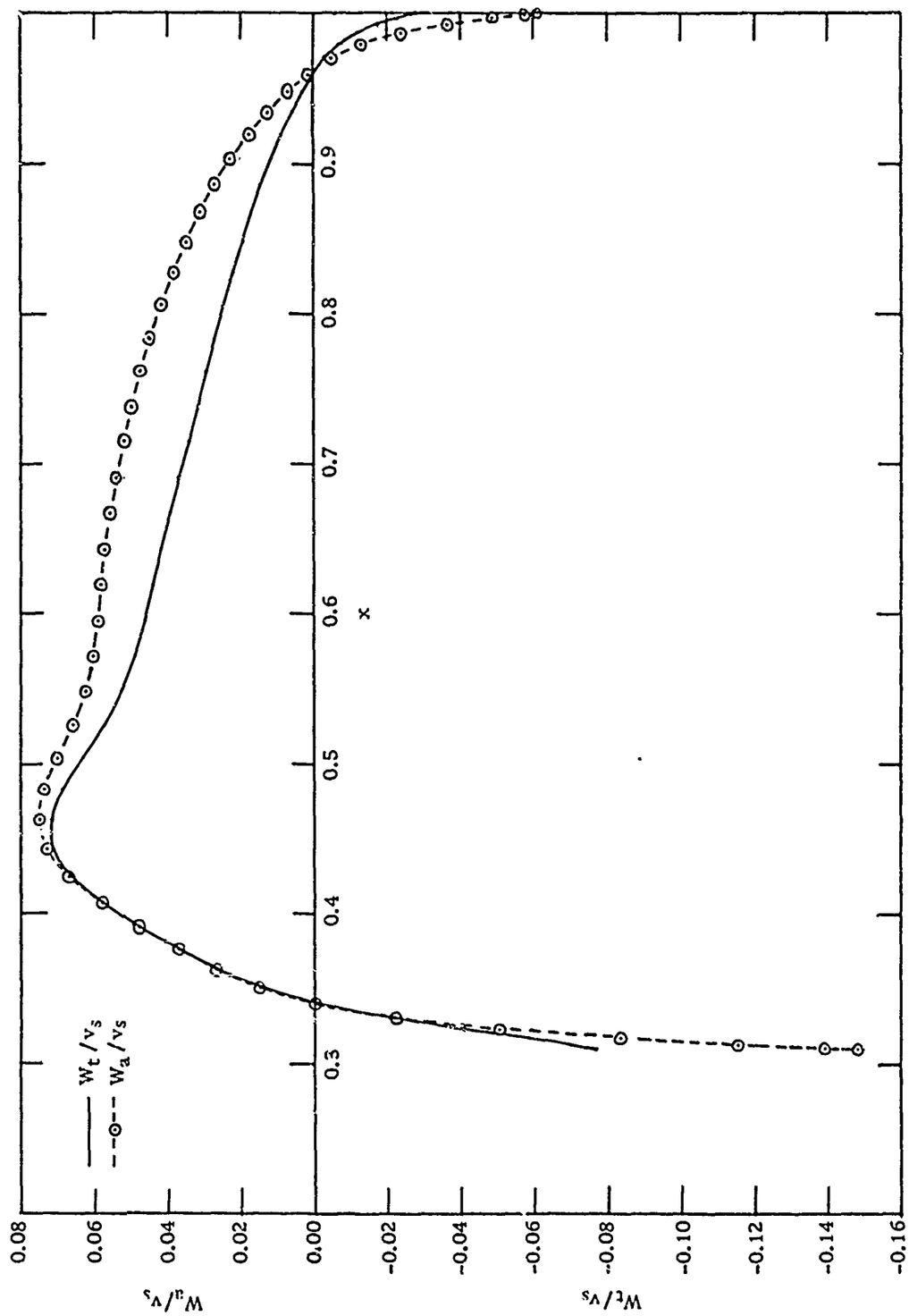

FIG. 9. Spanwise Variation of the Axial and Tangential Components of Induced Velocity at the Lifting Line.

solution, 14 terms were used in the odd Fourier expansion of the bound circulation and 16 terms in the even Fourier expansion of the induction factors. It is interesting to note that negative induced velocities occurred near the hub and the tip. Such a result is common for non-optimum propellers.

NORMAL COMPONENT OF INDUCED VELOCITY FROM LIFTING-SURFACE PROGRAMS

With the value of G_{max} and the pitch distribution

$$\beta = \arctan \frac{v_s' + W_a/v_s}{x/\lambda_s - W_t/v_s}$$

of the helical sheets given by the lifting-line solution, all the necessary inputs for the lifting-surface computer programs were made available. In the lifting-surface solution, it was assumed that the blades were not skewed and that the blade shape was symmetrical about the stacking line; i. e., $L = \frac{1}{2}C$ (see Fig. 3a, Ref. 1).

To illustrate the effect of operating in a wake, an identical lifting-surface solution (except that $x \tan\beta$ = CONSTANT = 0.456 was used) was carried along simultaneously with the lifting-surface solution for the wake-adapted propeller. The condition $x \tan\beta$ = CONSTANT is met exactly for lightly loaded free-running propellers, and approximately for moderately loaded free-running propellers. However, it is seriously violated for lightly or moderately loaded wake-adapted propellers operating in a wake profile of the turbulent boundary layer type. The value 0.456 corresponds to the magnitude of $x \tan\beta$ for the wake-adapted propeller at the center of the blade, $x = 0.65$.

The lifting-surface programs yield (1) the normal component of induced velocity resulting from the bound circulation, $(W_{\bar{Y}})_B$; (2) the difference resulting from the free vorticity between the normal component of induced velocity on the blade and the normal component of induced velocity at the lifting line from the lifting-line solution, $(W_{\bar{Y}})_F - (W_{\bar{Y}})_{FLL}$ (see discussion, Pages 30, 31, and 42, Ref. 1); and (3) the normal component of induced velocity resulting from blade thickness, $(W_{\bar{Y}})_T$. The variation of these normal components across the blade were calculated at three spanwise stations: (1) near the tip, $x = 0.9625$; (2) at the middle of the blade, $x = 0.65$; and (3) near the hub, $x = 0.37$.

A discussion of the width of the strips and the size of the singularity region used in these calculations is given in the Appendix.

Figure 10 shows the variation across the blade of the normal component of induced velocity resulting from the bound circulation, $(W_{\bar{Y}})_B$. It should be noted that these variations for both the case $x \tan\beta$ = CONSTANT and the wake-adapted case are odd functions about the half-chord position, $y = 0.5$. This results because there is no skew and because the blade shape and chordwise loading are symmetrical. If

the three conditions above are not met, the variation of $(W\bar{Y})_B$ over the front half of the blade will normally bear no simple relation to that over the rear half. A comparison of the magnitudes of $(W\bar{Y})_B$ between the case x tanβ = CONSTANT and the wake-adapted case shows that the effect of operating in the wake is essentially negligible near the tip and center of the blade, but produces significant differences near the hub.

Figure 11 shows the variation across the blade of $(W\bar{Y})_F - (W\bar{Y})_{FLL}$. Observe that these variations are odd functions about the half-chord position, y = 0.5, only for the case x tanβ = CONSTANT. Thus the blade must have not only symmetrical shape, symmetrical chordwise loading, and no skew, but also a constant x tanβ if $(W\bar{Y})_F - (W\bar{Y})_{FLL}$ is to satisfy this special relationship. If these conditions are not met, the variation of $(W\bar{Y})_F - (W\bar{Y})_{FLL}$ over the front half of the blade will generally bear no simple relation to that over the rear half. In comparing the magnitude of $(W\bar{Y})_F - (W\bar{Y})_{FLL}$ between the case x tanβ = CONSTANT and the wake-adapted case, it is seen that the effect of operating in the wake is small near the tip and center of the blade, but results in large differences near the hub, since the whole trend in the values is altered. Note also that the values of $(W\bar{Y})_F - (W\bar{Y})_{FLL}$ at the station near the tip (x = 0.9625) are reversed in sign compared to those at the center of the blade (x = 0.65). This reversal is related to the fact that the non-optimum circulation distribution (Fig. 6) yields negative values of induced velocity near the tip (Fig. 9).

The cross-blade variation of the normal component of induced velocity, which results from blade thickness, $(W\bar{Y})_T$, is given in Fig. 12. None of these curves show a simple relation between the variation over the front and rear halves of the blade. This is true for this propeller, and in general for all propellers, because thickness distributions of streamlined airfoil sections are not symmetric about the mid-chord position Comparing the magnitude of $(W\bar{Y})_T$ for the case x tanβ = CONSTANT with the wake-adapted case shows marked differences, not only near the hub, but also near the tip.

At this point, it is interesting to examine the reasons for the differences in behavior of the normal components of induced velocity for the case x tanβ = CONSTANT and the wake-adapted case. The normal components of induced velocity resulting from bound circulation and free vorticity were seen to be nearly the same for these two cases near the tip and center of the blade, but to differ considerably near the hub. This result is no surprise, considering the wake profile in which the propeller is operating. This profile (Eq. 4) is a reasonable approximation of a fairly full turbulent boundary layer. In such a profile, the variation in velocity in the outer portion is small, giving rise to small variations in x tanβ at the tip and middle of the blade. Near the hub, however, the variations in velocity are large, leading to large variations in x tanβ and consequently large differences between the x tanβ = CONSTANT and the wake-adapted cases there.

The differences between the two cases in the normal component of induced velocity resulting from blade thickness were seen to be

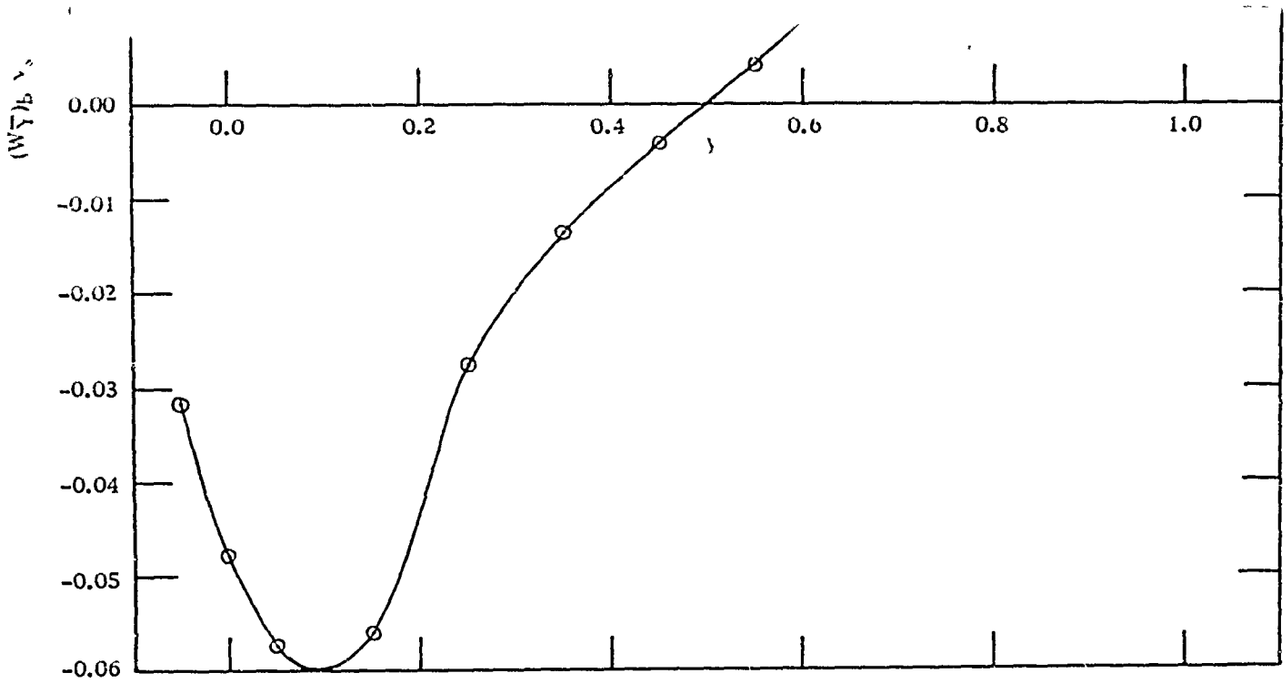

(b)

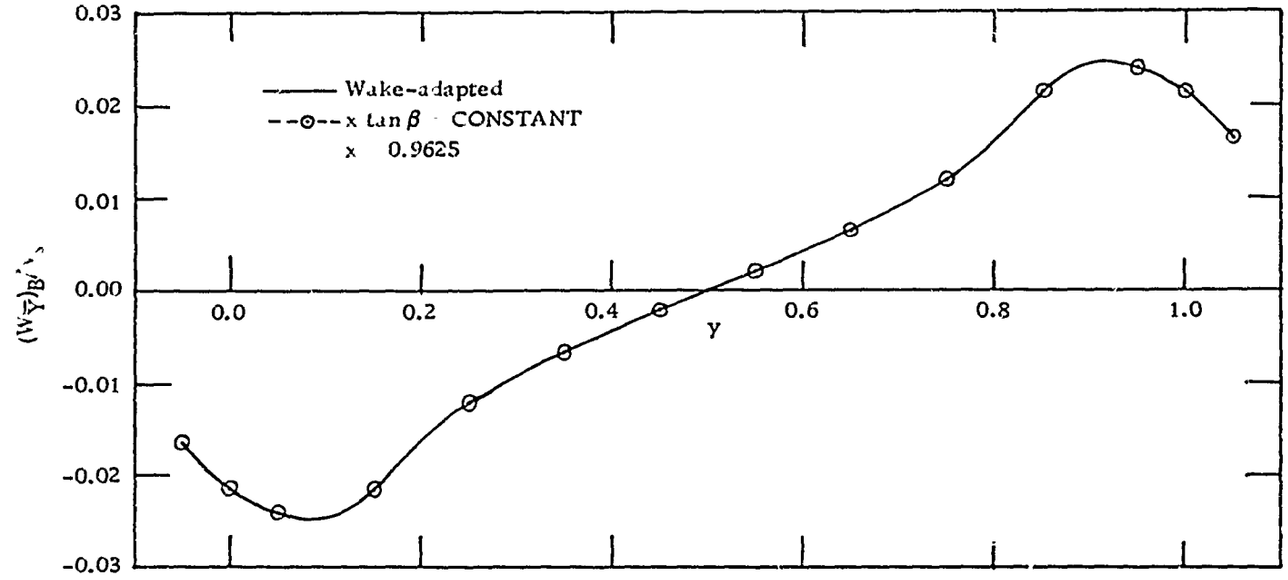

(c)

FIG. 10a - c. Chordwise Variation of the Normal Component of Induced Velocity Due to Bound Circulation at x = 0.37, 0.65, and 0.9625.

FIG. 12a - c Chordwise Variation of the Normal Component of Induced Velocity Due to Blade Thickness at x = 0.37, 0.65, and 0.9525.

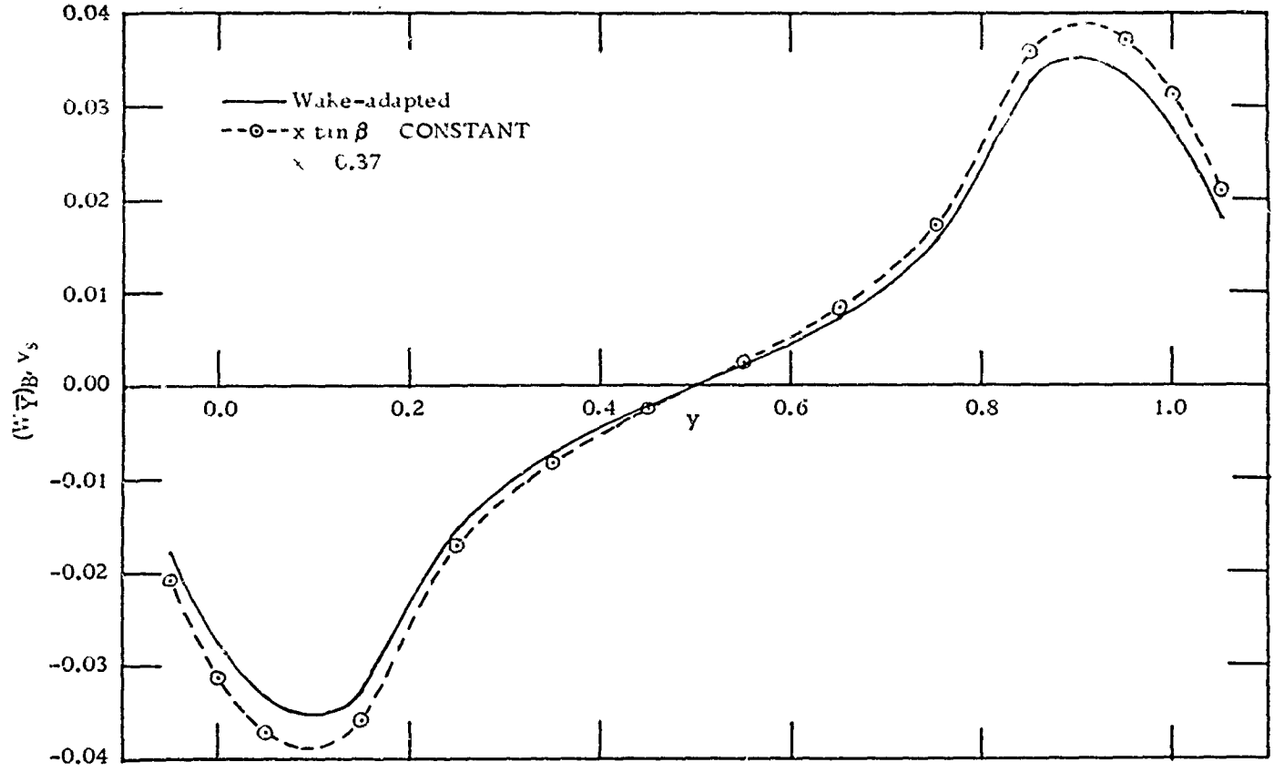

(a)

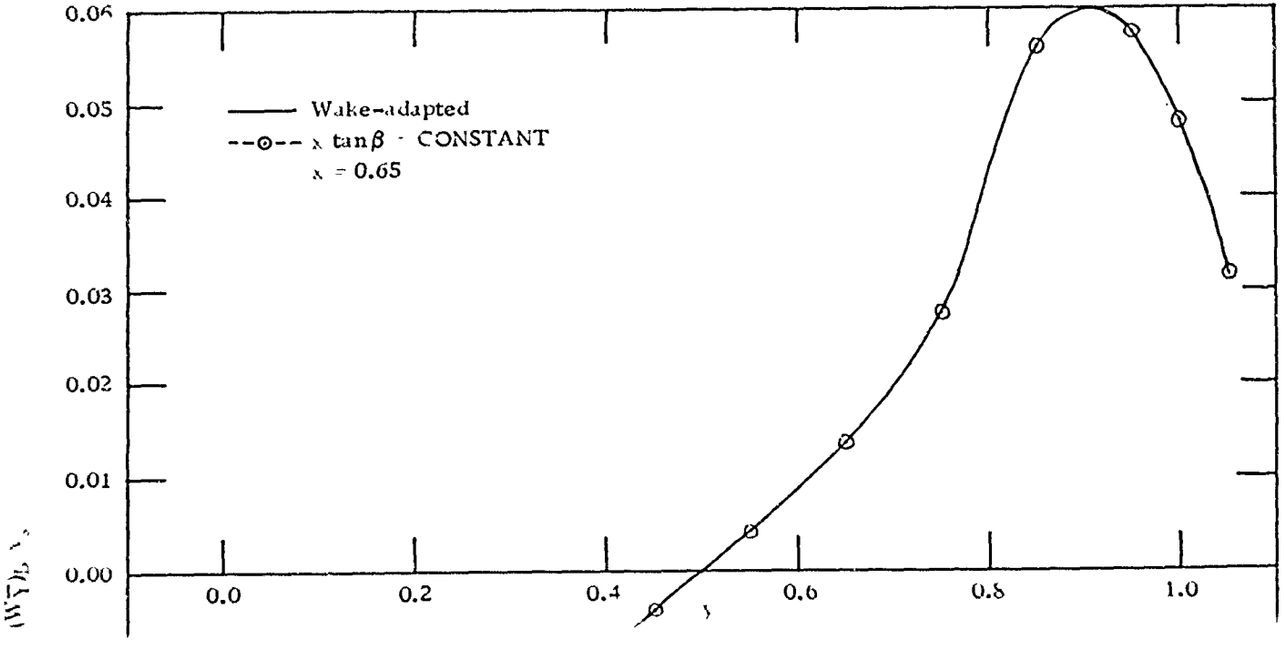

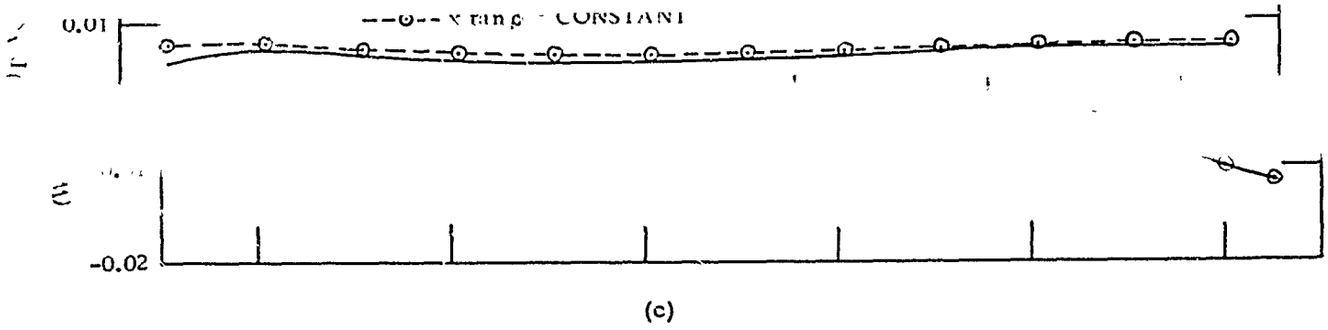

(c)

FIG. 11a - c. Chordwise Variation of the Normal Component of Induced Velocity Due to Free Vorticity at x = 0.37, 0.65, and 0.9625.

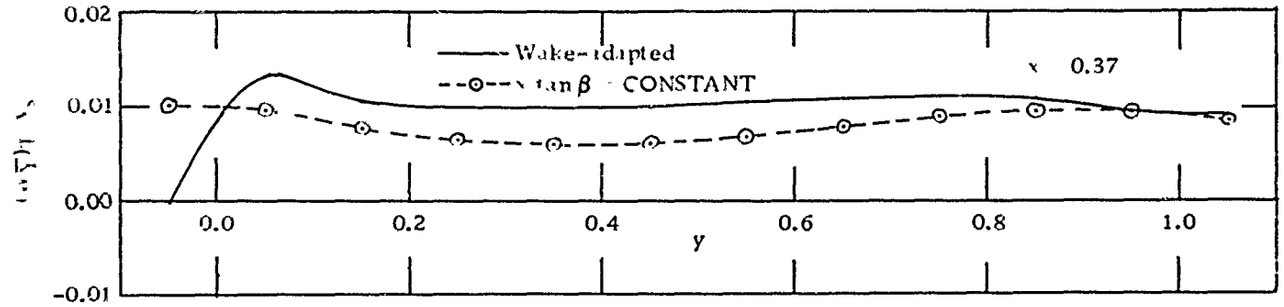

(a)

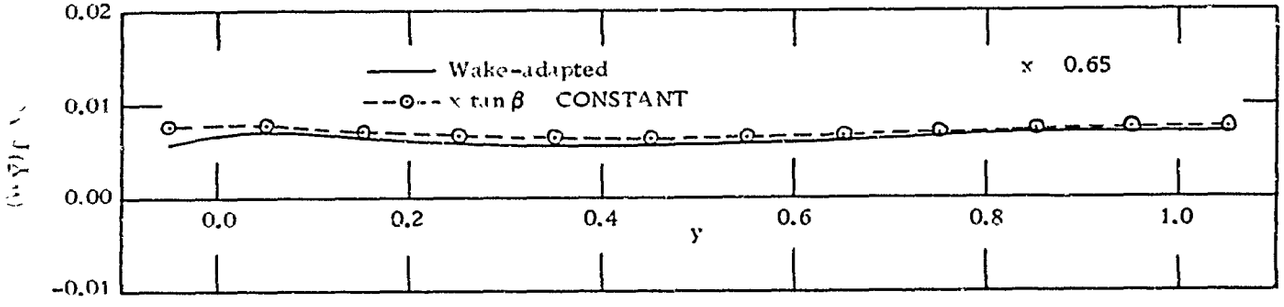

(b)

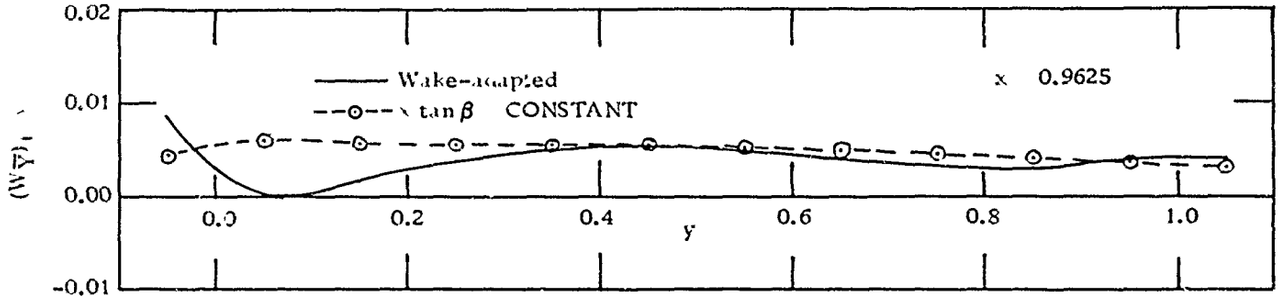

(c)

FIG. 12a - c Chordwise Variation of the Normal Component of Induced Velocity Due to Blade Thickness at x = 0.37, 0.65, and 0.9625.

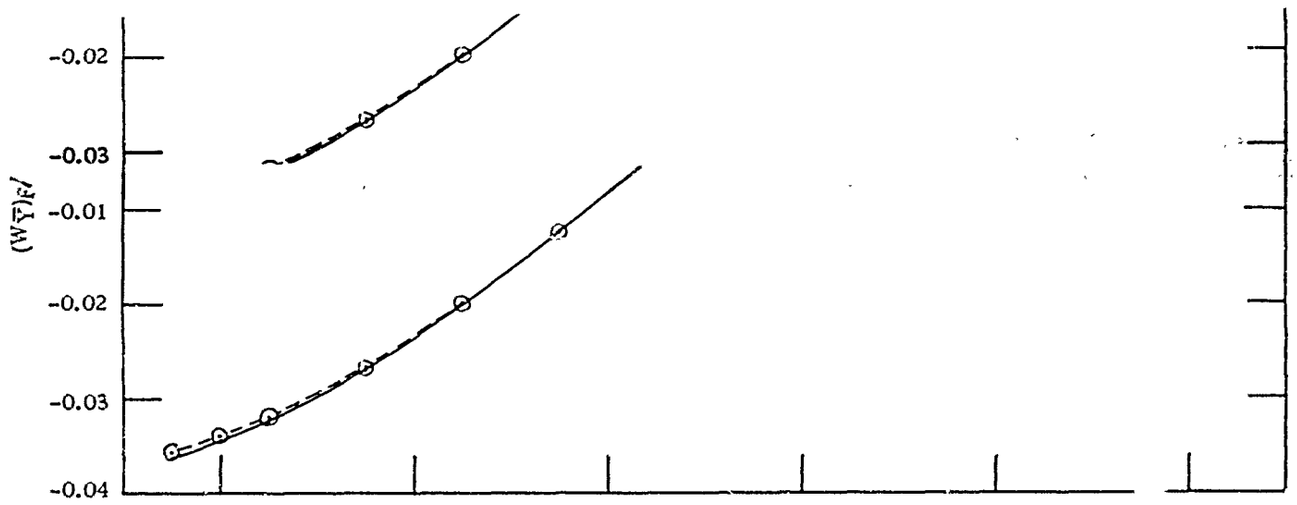

(b)

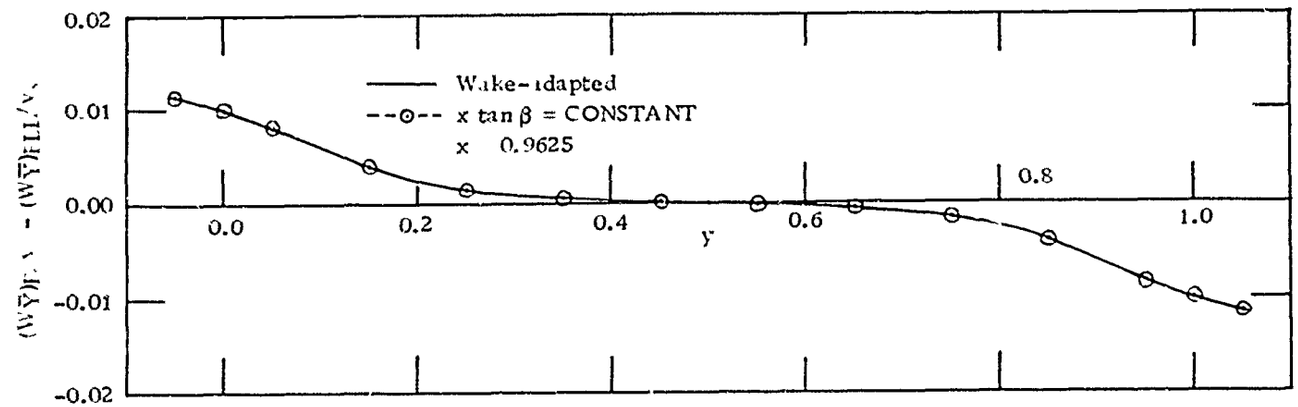

(c)

FIG. 11a - c. Chordwise Variation of the Normal Component of Induced Velocity Due to Free Vorticity at x = 0.37, 0.65, and 0.9625.

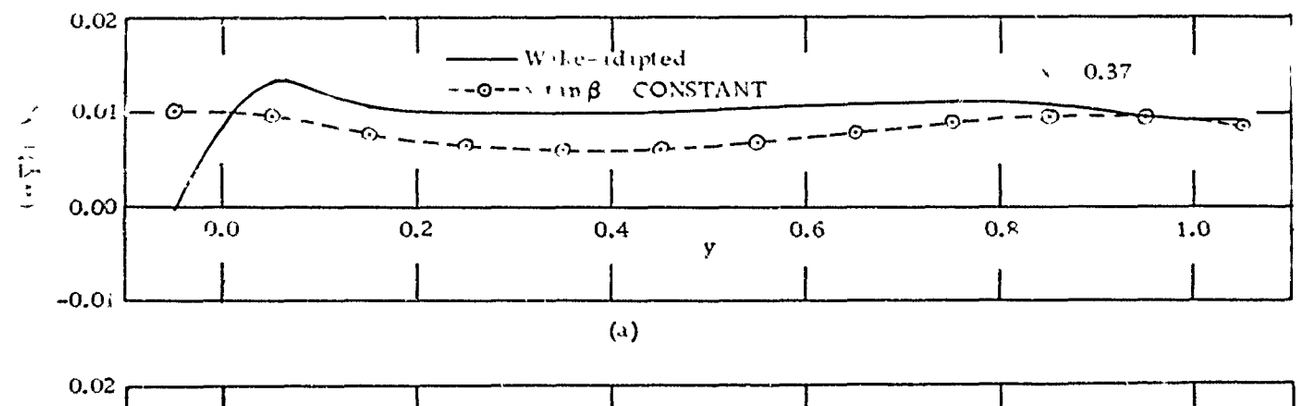

(a)

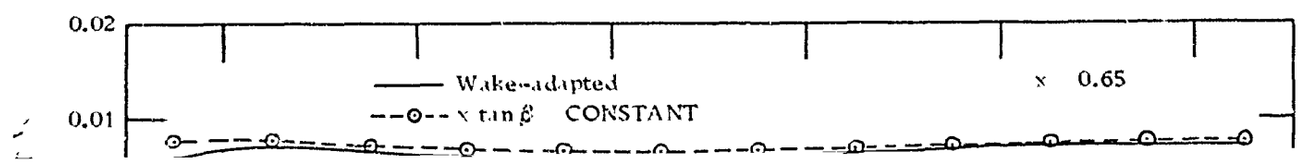

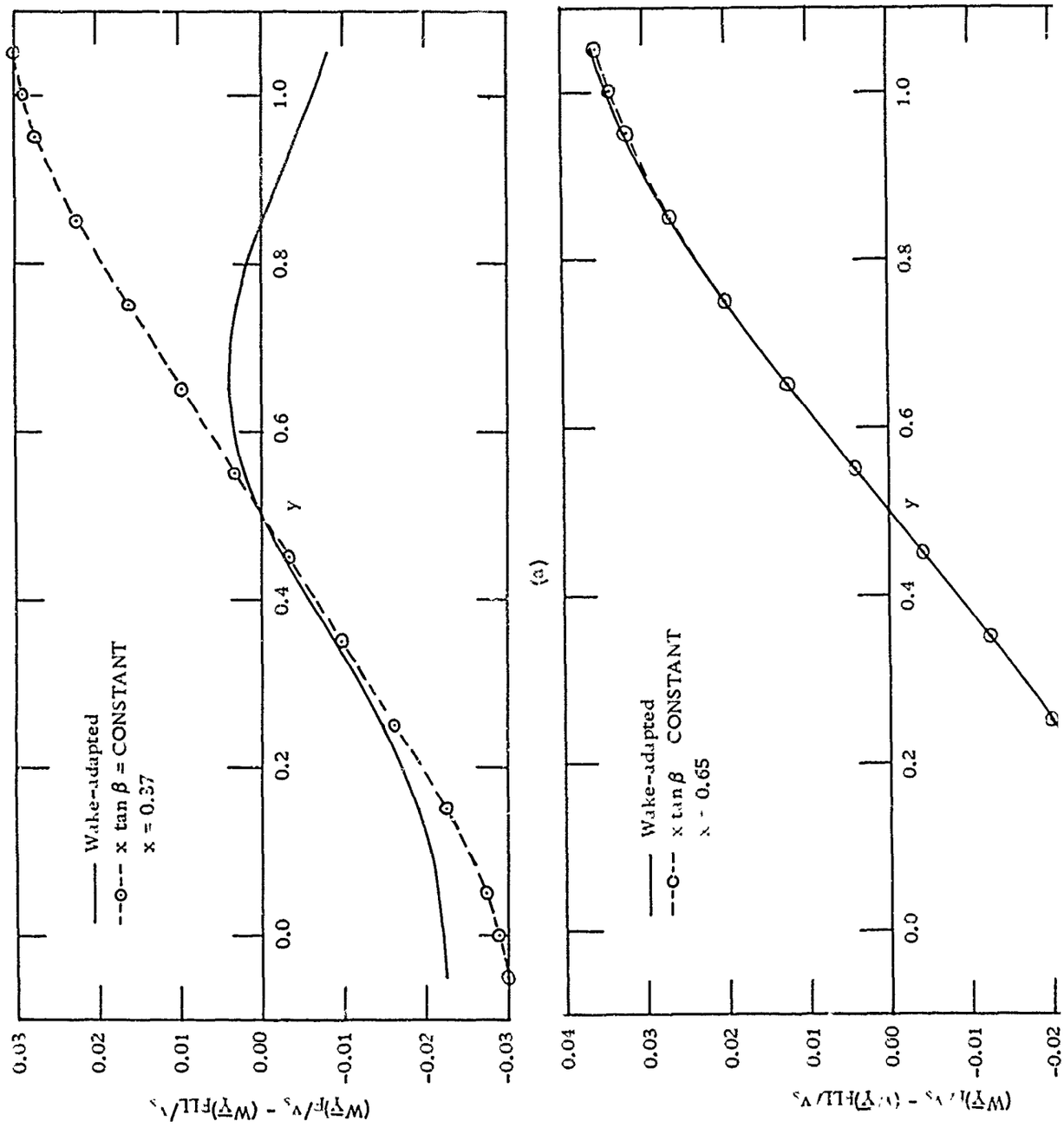
Wake-adapted
x tan β = CONSTANT
x = 0.37
y
0.0
0.2
0.4
0.6
0.8
1.0
0.03
0.02
0.01
0.00
-0.01
-0.02
-0.03
(W$\bar{\gamma}$)F/V$_s$ - (W$\bar{\gamma}$)FLL/V$_s$
(a)
Wake-adapted
x tan β CONSTANT
x = 0.65
0.04
0.03
0.02
0.01
0.00
-0.01
-0.02

relatively large not only near the hub, but also near the tip. This situation is not difficult to understand if one fact concerning blade thickness-induced flow is kept in mind. The $(W\bar{Y})_T$ velocity component normal to a line in the chordwise direction is not normal to a line in the spanwise direction if $x \tan\beta \neq$ CONSTANT. This can give rise to a much larger effect of a blade on itself for the wake-adapted case, compared to the case $x \tan\beta =$ CONSTANT. It is, in fact, the blades effect on itself that causes most of the differences seen in Fig. 12 at Stations $x = 0.37$ and $x = 0.9625$.

CAMBER LINES AND IDEAL ANGLES OF ATTACK

The camber lines and their orientation in the flow are determined from the variation of the normal component of induced velocity across the blade. A polynomial fit to the camber line slope is used to determine the camber line and its orientation, as discussed on Pages 42 and 43 of Ref. 1. In these calculations, the normal component of velocity used is

$$W\bar{Y} = (W\bar{Y})_B + (W\bar{Y})_F - (W\bar{Y})_{FLL} + (W\bar{Y})_T$$

where $(W\bar{Y})_{FLL}$ is the normal component of induced velocity at the lifting line from the lifting-line solution. Since this component is subtracted, the angle of attack γ (Eq. 49, Ref. 1) gives the orientation of the chord line in relation to the relative flow velocity vector at the lifting line as shown in Fig. 13. This angle, γ, is analogous to the ideal angle of attack for two-dimensional camber lines, and will be referred to by that name.

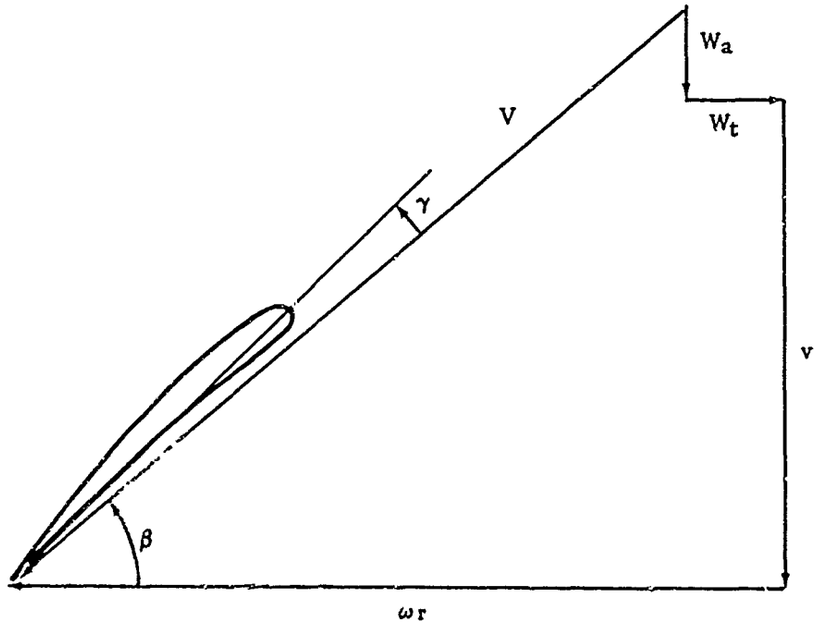

FIG. 13. Velocity Diagram Showing Blade Orientation Relative to Flow at the Lifting Line.

Figure 14 shows the camber lines and ideal angles of attack where the blade thickness effect has been neglected. For the case $x \tan\beta$ = CONSTANT, the camber lines are symmetrical about the half-chord position, $y = 0.5$, and the ideal angles of attack are all zero. This results because the normal components of induced velocity from bound circulation and free vorticity (Fig. 10 and 11) are odd functions about the half-chord position. Recall that this relationship occurred because there was no skew, the blade shape and chordwise loading were symmetrical, and $x \tan\beta$ equalled a constant. For the wake-adapted case, it is seen that, in general, the camber lines are not symmetrical about the half-chord position and the ideal angles of attack are not zero, even if the blade thickness is negligible.

The calculated camber lines and ideal angles of attack, including the blade thickness effect, are shown in Fig. 15. Since the variation of the normal component of induced velocity from blade thickness over the front half of the blade bears no simple relation to that over the rear half (Fig. 12), the camber lines are not symmetric about the half-chord position, and the ideal angles of attack are not zero, regardless of whether $x \tan\beta$ = CONSTANT. A comparison of Fig. 14 and 15 shows that while the blade thickness-induced velocity field yields a distortion of the camber lines, its principal effect is to alter the ideal angles of attack. These alterations are as large as 0.606°.

SIGNIFICANT FEATURES OF TYPICAL DESIGN CALCULATIONS

In the foregoing typical design calculations for a wake-adapted propeller, one feature stands out. For propellers operating in a wake of the turbulent boundary layer type, the radial variation of $x \tan\beta$ must be accounted for in the design calculation if anything approaching correct results are to be obtained. Hence the assumption made in Ref. 4 that this variation gives rise to negligible effects is apparently not justified in the design of propellers for bodies such as torpedoes or submarines where the inflow velocity profile is typically that of a turbulent boundary layer. Furthermore, it is doubtful that satisfactory values of the normal component of induced velocity due to blade thickness for a wake-adapted propeller can be obtained where the radial variation of $x \tan\beta$ is neglected as proposed in Ref. 2.

The foregoing calculations have also shown that the alteration in ideal angle of attack resulting from blade thickness is sufficiently large, even for propellers having only five blades, that the effects of such thickness must be included in propeller design.

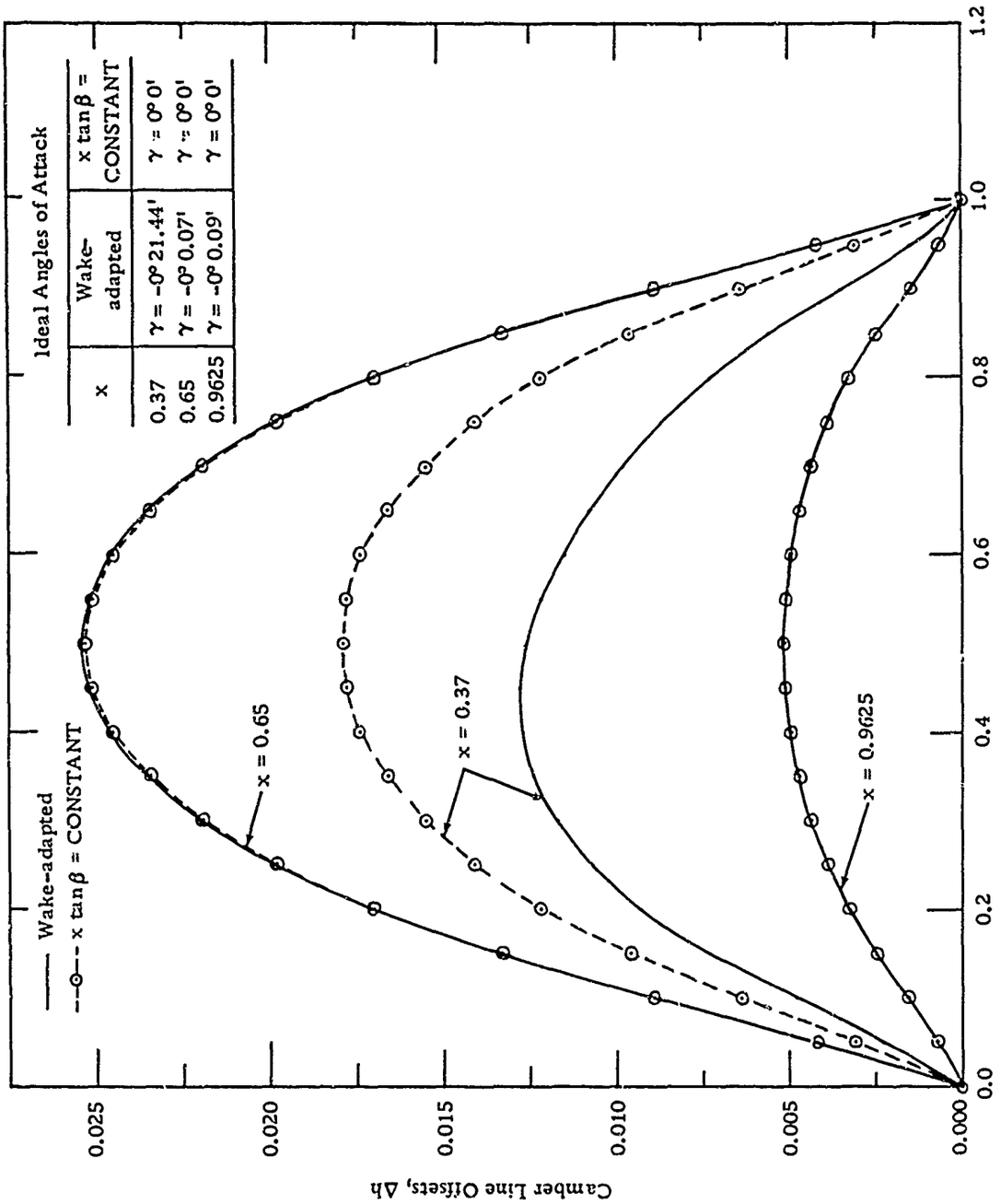

FIG. 14. Camber Lines and Their Orientation Neglecting Blade Thickness.

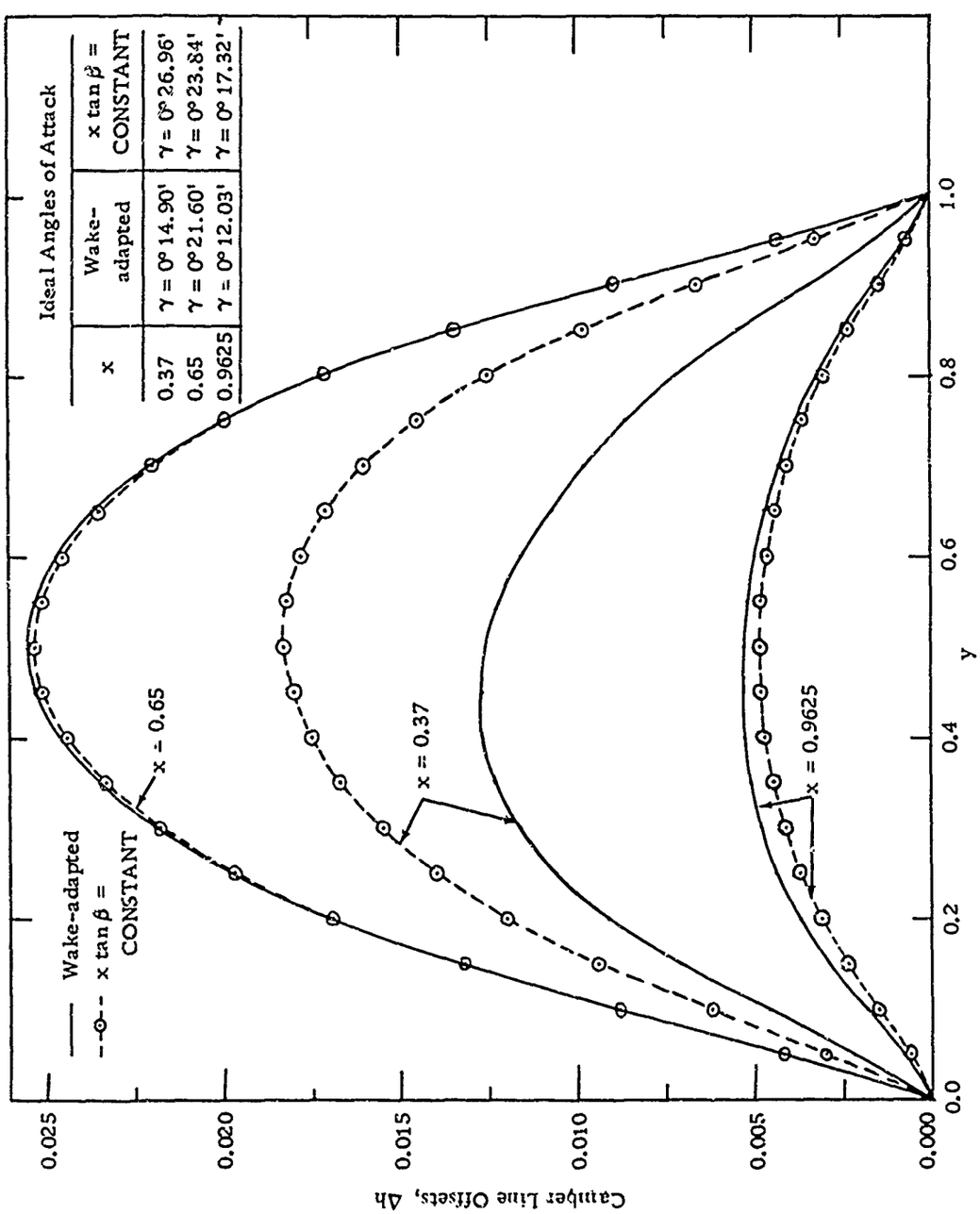

FIG. 15. Camber Lines and Their Orientation, Including Blade Thickness.

CHANGES AND ADDITIONS TO THE LIFTING-SURFACE PROPELLER DESIGN METHOD

MODIFICATIONS TO LIFTING-SURFACE PROGRAMS

Several small modifications, not included in Ref. 1, were made to the lifting-surface propeller design programs. The tests shown on Pages 15, 16, 29, 39, and 40 of Ref. 1 on the quantity $4ac - b^2$ to determine the expression for Q to use were changed to

$$|4ac - b^2| > 0.01b^2 \qquad \text{and} \qquad |4ac - b^2| \lesssim 0.01b^2$$

By means of this alteration, the test was made independent of the blade shape and the accuracy of the solutions were improved.

To make the approximation to k (see bottom of Page 33, Ref. 1) across the singularity region equal in accuracy regardless of the spanwise position, the value of $\Delta\alpha$ (Fig. 11, Ref. 1) is computed so that the distance across the region is a constant percent chord, ΔY. Thus

$$\Delta\alpha = f_{3p}\Delta Y$$

The lifting-surface programs do not allow the normal component of induced velocity to be computed directly at the leading or trailing edge of the blade. Hence values were computed at points off the leading and trailing edges, y = -0.05 and 1.05. Thus the values normally used in computing a camber line corresponded to y = -0.05, 0.05, 0 15, 0.25, 0.35, 0.45, 0.55, 0.65, 0.75, 0.85, 0.95, and 1.05. As a result of the often-encountered peculiar behavior of polynomial fits to a set of points near the end points, it was found that the accuracy of the camber line program could be enhanced by interpolating values of the normal component of induced velocity at the leading and trailing edge (y = 0.0 and 0.1) using a three-point Lagrange method. These two new values, plus the original twelve listed above, are all used in computing the camber lines. Further, it was found that writing the power series representing the camber line about the half-chord position also improved the accuracy of the camber line program. Thus

$$h = a_0 + a_1\bar{y} + a_2\bar{y}^2 + a_3\bar{y}^3 + \cdots a_j\bar{y}^j$$

where $\bar{y} = y - 0.5$. Equation 49 of Ref. 1 now becomes

$$\gamma = \sum_{i=1}^{j} a_i(\bar{y}_{LE}^i - \bar{y}_{TE}^i)$$

$$\Delta h = (\bar{y} - \bar{y}_{TE})\gamma + (\bar{y} - \bar{y}_{TE})a_1 + (\bar{y}^2 - \bar{y}_{TE}^2)a_2 + \cdots \quad (\bar{y}^j - \bar{y}_{TE}^j)a_j$$

where $\bar{y}_{LE}$ and $\bar{y}_{TE}$ are the values of $\bar{y}$ at the leading and trailing edges: -0.5 and 0.5, respectively.

ADDITION OF THE HUB BOUNDARY CONDITION

Extension of the Douglas Potential Flow Program. It was mentioned in Ref. 1 that the hub boundary condition can be included in propeller design by using a surface source density over the hub boundary. Hess and Smith (Ref. 10) worked out a method for computing the potential flow about an arbitrary body in a uniform onset flow using the surface source density approach. Recently this work was extended,[4] so that an arbitrary onset flow may be considered. However, the capability of computing velocities at off-body points was not included in the computer program. At the present time, the Douglas Aircraft Co., under contract to NOTS, is extending the program to include the capability of computing velocities at off-body points. With these extensions, the inclusion of the hub boundary condition by means of the Douglas computer program becomes a relatively simple task.

Use of the Douglas Program in the Propeller Hub Problem. In the method developed by Hess and Smith for computing the potential flow about arbitrary bodies, the body is represented by a patchwork of four-sided plane elements over which the source density is assumed constant. The source density strength of each element is determined by the condition that no fluid must penetrate the boundary. This boundary condition is satisfied at the center of each element. In the extended program, it is possible to specify an arbitrary normal component of onset flow in satisfying the boundary condition. Hence the condition that fluid not penetrate the boundary can be met even if the body is in the presence of a disturbance such as that created by a propeller.

Using the surface source patchwork to represent the propeller hub, it is first necessary to compute the normal component of velocity induced by the propeller at the center of each element. Using these values in the Douglas program, the source densities needed to satisfy the hub boundary condition can be determined and the velocities induced by the hub at one propeller blade can be computed. The hub-induced velocities can then be incorporated into the calculation of the camber lines and ideal angles of attack of the propeller blade sections. The pitch of the blade section chord lines may be significantly altered by the hub-induced velocities, so that the blades do not lie close to the helical sheets upon which the blades were initially assumed to lie when the normal component of velocity at the hub was computed. In such a case, it may be necessary to iterate the solution correcting the pitch distribution of the helical sheets. It is probable, however, that such a procedure will not be necessary.

Calculation of the Propeller-Induced Normal Component of Velocity at the Hub. In Ref. 1, the subscript p was used to define the singularity point on the blade where the normal component of induced velocity was

---

[4] Douglas Aircraft Co., Inc. "Three-Dimensional Potential Flow for Non-Uniform Onset Flow," by G. E. Short. Douglas Aircraft Div., Long Beach, Calif., September 1964. (Memorandum C1-210-TM-26D.)

desired. In this section, the subscript p is used to define the point on the hub where the component of velocity normal to the hub is desired.

Using a helical coordinate system to define this point, the coordinates in the X', Y', Z' system (see Fig. 1, Ref. 1) of point p are given by Eq. 1, Ref. 1.

$$\begin{aligned} X'_p &= \alpha_p r_h \tan\beta_h \\ Y'_p &= -r_h \sin(\psi_p + \alpha_p) \\ Z'_p &= r_h \cos(\psi_p + \alpha_p) \end{aligned} \tag{7}$$

The value of β_h to be used, and the reason for using a helical coordinate system to locate point p, will be discussed later.

Making this Eq. 7 nondimensional by use of Eq. 7, Ref. 1, one obtains

$$\begin{aligned} X_p &= \alpha_p x_h \tan\beta_h \\ Y_p &= -x_h \sin(\psi_p + \alpha_p) \\ Z_p &= x_h \cos(\psi_p + \alpha_p) \end{aligned} \tag{8}$$

A rectangular $\underline{X}'$, $\underline{Y}'$, $\underline{Z}'$ coordinate system is defined as shown in Fig. 16. The $\underline{X}'$ axis coincides with the X' axis, and the $\underline{Z}'$ axis passes through point p on the hub normal to the hub surface.

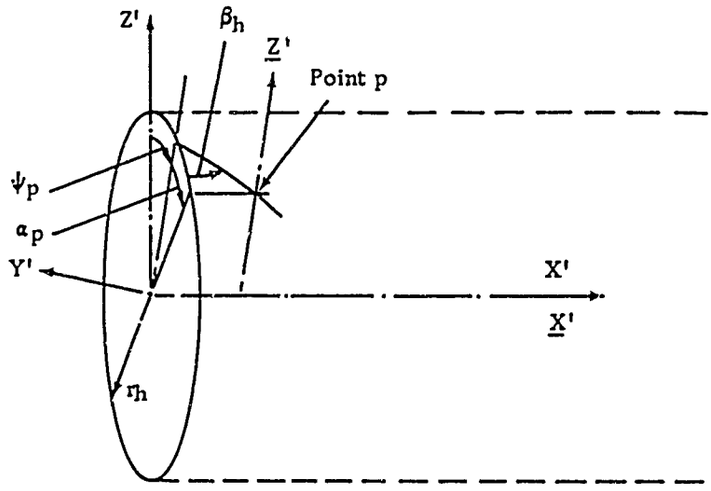

FIG. 16. Rectangular $\underline{X}'$, $\underline{Y}'$, $\underline{Z}'$ Coordinate System.

A vector having components A_X, A_Y, A_Z in the X', Y', Z' coordinate system will have components in the $\underline{X}'$, $\underline{Y}'$, $\underline{Z}'$ system given by

$$A_{\underline{X}} = A_X$$

$$A_{\underline{Y}} = A_Y \cos(\psi_p + \alpha_p) + A_Z \sin(\psi_p + \alpha_p) \tag{9}$$

$$A_{\underline{Z}} = -A_Y \sin(\psi_p + \alpha_p) + A_Z \cos(\psi_p + \alpha_p)$$

Looking first at the normal component of velocity at the hub induced by the bound circulation, the Biot-Savart law (Eq. 14, Ref. 1) is used to compute the desired velocity. The component of velocity normal to the hub will be in the $\underline{Z}'$ direction (see Fig. 16). Hence Eq. 14, Ref. 1, gives

$$W_{\underline{Z}} = \frac{1}{4\pi} \int_\ell \overline{\Gamma} \frac{S_{\underline{Y}} d\ell_{\underline{X}} - S_{\underline{X}} d\ell_{\underline{Y}}}{S^3} \tag{10}$$

Replacing Eq. 15, Ref. 1, with Eq. 10 and using Eq. 7 in an analysis similar to that carried out on Pages 6 - 17 of Ref. 1, it is easily shown that the right-hand side of Eq. 19, Ref. 1, yields the nondimensional normal component of induced velocity at the hub due to the bound circulation $(W_{\underline{Z}})_B / v_s$ if

$$A_0 = -(X_p - y_n f_1 + f_2)[f_8 - f_4 - y_n(f_7 - f_3)] \cos(\psi_m + y_n f_3 - f_4 - \psi_p - \alpha_p)$$
$$+ [(y_n f_5 - f_6)x + (X_p - y_n f_1 + f_2)] \sin(\psi_m + y_n f_3 - f_4 - \psi_p - \alpha_p)$$

$$A_1 = \{(y_n f_5 - f_6)x f_3 + f_1[f_8 - f_4 - y_n(f_7 - f_3)] + (X_p - y_n f_1 + f_2) f_7\}$$
$$\cos(\psi_m + y_n f_3 - f_4 - \psi_p - \alpha_p)$$
$$+ \{x f_5 - f_1 + (X_p - y_n f_1 + f_2)[f_8 - f_4 - y_n(f_7 - f_3)] f_3\}$$
$$\sin(\psi_m + y_n f_3 - f_4 - \psi_p - \alpha_p)$$

$$A_2 = (x f_3 f_5 - f_1 f_7) \cos(\psi_m + y_n f_3 - f_4 - \psi_p - \alpha_p)$$
$$- \{[f_8 - f_4 - y_n(f_7 - f_3)] f_1 f_3 + (X_p - y_n f_1 + f_2) f_3 (f_7 - f_3)\}$$
$$\sin(\psi_m + y_n f_3 - f_4 - \psi_p - \alpha_p)$$

$$A_3 = f_1 f_3 (f_7 - f_3) \sin(\psi_m + y_n f_3 - f_4 - \psi_p - \alpha_p)$$

$$\epsilon = 0$$

$$(\Delta W_{\bar{Y}})_B / v_s = 0$$

and X_p, Y_p, and Z_p are given by Eq. 8.

Note that ϵ and ΔW are zero, since no singularity will appear in the solution if the boundaries of the surface source elements representing the hub are properly chosen (as will be discussed later).

Similar analyses show that

1. The right-hand side of Eq. 35, Ref. 1, yields the nondimensional normal component of induced velocity at the hub due to free vorticity, $(W_{\underline{Z}})_F/v_s$, if

$$A_0 = x_n M_n \sin(\psi_m + \alpha - \psi_p - \alpha_p) + (X_p - \alpha M_n) x_n \cos(\psi_m + \alpha - \psi_p - \alpha_p)$$

$$A_1 = (M_n + x_n N_n) \sin(\psi_m + \alpha - \psi_p - \alpha_p) + [X_p - \alpha(M_n + x_n N_n)] \cos(\psi_m + \alpha - \psi_p - \alpha_p)$$

$$A_2 = N_n[\sin(\psi_m + \alpha - \psi_p - \alpha_p) - \alpha \cos(\psi_m + \alpha - \psi_p - \alpha_p)]$$

$$\epsilon = 0$$

$$(\Delta W_{\overline{Y}})_F/v_s = 0$$

and X_p, Y_p, and Z_p are given by Eq. 8.

2. The right-hand side of the equation[5] on Page 39 of Ref. 1 yields the nondimensional normal component of the induced velocity at the hub due to the blade thickness, $(W_{\underline{Z}})_T/v_s$, if

$$A_0 = x_h - x \cos(\psi_m + y_n f_3 - f_4 - \psi_p - \alpha_p)$$

$$A_1 = x f_3 \sin(\psi_m + y_n f_3 - f_4 - \psi_p - \alpha_p)$$

$$\epsilon = 0$$

$$(\Delta W_{\overline{Y}})_T/v_s = 0$$

and X_p, Y_p, and Z_p are given by Eq. 8.

Thus it is seen that small additions to the computer programs, already developed to determine the component of induced velocity normal to the propeller blade, will give them the capability of determining the component normal to the hub. Work to add this capability to the programs has been started.

Arrangement of Surface Source Elements on the Hub. In order that no singularities or near-singularities occur in the calculation for the normal component of velocity induced at the hub by the propeller, it is necessary to arrange the surface source elements on the hub so that none of their midpoints fall on or near the intersection of the hub and the singularity sheets representing the propeller. This can be done by

[5] The equation referred to was not given a number in Ref. 1. It is the expression for $(W_{\overline{Y}})_T/v_s$.

dividing the hub surface by planes X' = CONSTANT perpendicular to the axis and by helical lines on the hub surface at a pitch angle β_h, which is the angle of the propeller helical sheets at the hub. This arrangement is shown in Fig. 17.

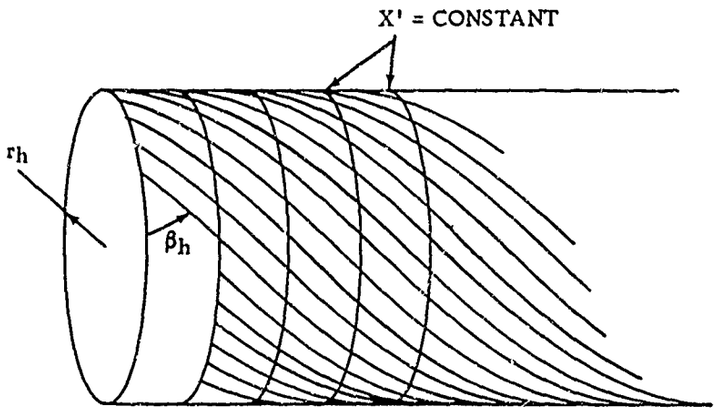

FIG. 17. Arrangement of Surface Source Elements on the Hub.

By having a helical source element boundary coincide with the intersection of the hub and each of the propeller helical sheets, the points where the normal component of velocity is computed will be at least one-half element width away from the propeller singularity sheets.

An additional advantage of the arrangement shown in Fig. 17 is that the angular periodicity of the propeller's induced velocity field may be exploited so that propeller-induced normal components of velocity at the hub need be calculated over only 1/g (g = number of blades) of the hub surface.

Because of the limitation in the number of elements the Douglas program can handle (maximum: 1,000 points defining the corners of the elements), it will be necessary (1) to accurately represent the hub in the vicinity of the propeller by using a large number of small elements in that region; (2) to less accurately represent the hub at more distant points in front and behind the propeller by using fewer, larger elements; and (3) to ignore the hub boundary condition altogether at points three to four propeller diameters in front of and behind the propeller. Since the velocity induced by a source falls off as the inverse square of the distance, such a representation will give accurate values for the hub-induced velocity at the propeller.

CONCLUSIONS

Check solutions of the lifting-surface design programs indicate that these programs can yield a level of accuracy which is more than adequate for engineering design calculations. The discussion in the Appendix points out that this level of accuracy can be achieved with moderate computing times.

The typical design calculations point out two important features of propeller-induced flow:

1. For propellers operating in a wake profile of the turbulent boundary layer type, it is essential that the radial variation of $x \tan\beta$ be accounted for in the lifting-surface calculations if anything approaching correct results are to be obtained. The errors induced by neglecting this variation occur principally near the hub when computing the effect of bound circulation and free vorticity. However, significant errors may occur, both near the hub and the tip, when computing the effect of blade thickness. Hence the radial variation of $x \tan\beta$ appears to be an important factor in the design of propellers for torpedoes and submarines where the propellers typically operate in a turbulent boundary layer wake profile.

2. The effect of blade thickness, even for a propeller having only five blades, is sufficiently large that it should be included in propeller design. The blade thickness-induced velocity field causes a distortion of the camber lines, but its principal effect is an alteration in the ideal angles of attack or pitch distribution of the blade sections. These are essentially the conclusions arrived at by Kerwin and Leopold in Ref. 3.

Once the hub boundary condition has been incorporated into lifting-surface propeller design, all parts of the propeller system will be quite accurately represented by the theoretical singularity distribution model. Most likely, the theoretical aspects of single-rotating propeller design will then be carried as far as is presently reasonable from a practical standpoint. Experimental work aimed at (1) determining better viscous corrections to lift, and (2) obtaining better viscous corrections to ideal angle of attack for propeller blade loadings having good cavitation resistance, might then round out the engineering design of single-rotating propellers.

Appendix

WIDTH OF STRIPS AND SIZE OF SINGULARITY REGION

In the check solutions and the typical design calculations presented here, the width of the strips and size of the singularity region (see discussion, Page 5, Ref. 1) used in the lifting-surface computer programs were determined by a compromise between accuracy and computing time. The solutions obtained by the programs become more accurate as the strips are made narrower and the singularity region made smaller, until the numerical accuracy of the computer breaks down due to the number of significant figures retained. However, this increased accuracy must be paid for in increased computation time and cost. Therefore, when the width of the strips and size of the singularity region have been made small enough to obtain the level of accuracy needed for engineering design calculations, the added cost of more accurate solutions is wasted, since the differences cannot be fabricated into the propeller. The list below, based on the check solutions and design calculations run to date, gives the strip widths and singularity region sizes for the various programs that should yield answers accurate within a small fraction of 1%. Using these values, about 22 minutes of IBM 7094 computer time is required to determine the camber line and ideal angle of attack for one blade station. Based on the current cost of computer time at NOTS, the computer cost for a complete propeller design would be approximately $850.

1. Bound Circulation Program.

   Number and width of strips: Ten of equal width, $\Delta Y = 0.1$.
   Length of singularity region: $\Delta X = 0.02$.

2. Free Vorticity Program.

   Number and width of strips: Sixteen to twenty, varying from $\Delta X = 0.02$ to $\Delta X = 0.10$. The distribution of these strips cannot be specified in advance for a given propeller, but must be chosen to represent accurately the radial variation of $x \tan\beta$, the chord, and the circulation.
   Length of singularity region: $\Delta Y = 0.02$.

3. Blade Thickness Program.

Number and width of strips:	Twelve, three at the leading edge of width $\Delta Y = 0.3333$, the remainder of width $\Delta Y = 0.1$. The three narrow strips at the leading edge are required to represent adequately the rapid change in thickness which occurs at that location for nearly all practical thickness distributions.
Length of singularity region:	$\Delta X = 0.01$.

REFERENCES

1. U. S. Naval Ordnance Test Station. A Lifting-Surface Propeller Design Method for High-Speed Computers, by D. M. Nelson. China Lake, Calif., NOTS, January 1964. (NAVWEPS Report 8442, NOTS TP 3399.)
2. Massachusetts Institute of Technology, Department of Naval Architecture and Marine Engineering. Linearized Theory for Propellers in Steady Flow, by J. E. Kerwin. Cambridge, Mass., MIT, July 1963.
3. Kerwin, J. E., and R. Leopold. "Propeller-Incidence Correction Due to Blade Thickness," J SHIP RES, Vol. 7, No. 2 (October 1963), pp. 1 - 6.
4. David Taylor Model Basin. Hydrodynamic Aspect of Propeller Design Based on Lifting-Surface Theory; Part I: Uniform Chordwise Load Distribution, by H. M. Cheng. Washington, D. C., DTMB, September 1964. (Report 1802.)
5. Pien, Pao C. "The Calculation of Marine Propellers Based on Lifting-Surface Theory," J SHIP RES, Vol. 5, No. 2 (September 1961), pp. 1 - 14.
6. Goldstein, S. "On the Vortex Theory of Screw Propellers," ROY SOC LONDON, PROC, Series A, Vol. 63, 1929.
7. Betz, Albert. "Schraubenpropeller mit geringstem Energieverlust," GOETTINGER NACHR, 1919.
8. Lerbs, H. W. "Moderately Loaded Propellers With a Finite Number of Blades and an Arbitrary Distribution of Circulation," SOC NAVAL ARCH MARINE ENGR, TRANS, Vol. 60, 1952.
9. U. S. Naval Ordnance Test Station. Slender-Airfoil Camberlines With Trapezoidal Lift Distribution, by M. L. Sturgeon. China Lake, Calif., NOTS, June 1963. (NAVWEPS Report 8092, NOTS TP 3145.)
10. Douglas Aircraft Co., Inc. Calculation of Non-Lifting Potential Flow About Arbitrary Three-Dimensional Bodies, by J. L. Hess and A. M. O. Smith. Long Beach, Calif., Douglas Aircraft Div., March 1962. (Report E. S. 40622.)